2019-01-01

Role of waves and tides on depth of closure and potential for headland bypassing

Valiente, NG

10.1016/j.margeo.2018.10.009
Marine Geology
Elsevier

Marine Geology 407 (2019) 60–75

Contents lists available at ScienceDirect

Marine Geology

journal homepage: www.elsevier.com/locate/margo

Role of waves and tides on depth of closure and potential for headland bypassing

Nieves G. Valiente*, Gerd Masselink, Tim Scott, Daniel Conley, Robert Jak McCarroll

Coastal Processes Research Group, School of Biological and Marine Sciences, Plymouth University, PL4 8AA, UK

ARTICLE INFO

Editor: Edward Anthony

Keywords:
Nearshore sediment transport
Bed shear stress
Depth of closure
Headland bypassing
Macrotidal
Embayments

ABSTRACT

Depth of closure is a fundamental concept used to define the seaward extent of a morphodynamically active shoreface at a particular temporal scale. The estimation of this limit in relation to the depth in front of the bounding headlands along embayed coastlines allows questioning whether embayments, often deemed closed sediment cells, experience more headland bypassing than expected. Wave-based parameterisations developed for microtidal beaches are most widely used to estimate closure depth; however, a re-evaluation of the concept for shorefaces influenced by geological control (presence of headlands and/or bedrock) and strong tidal currents is appropriate. Here, we use the macrotidal, embayed and high-energy coastline of SW England to identify the 'active' nearshore limits with a multi-method approach that includes observations of shoreface morphology and sedimentology, offshore/inshore wave formulations and bed shear stress computations. We identify the basal limit of 'significant' (i.e., 0.14 m) morphological change (Depth of Closure; *DoC*) and a maximum depth of extreme bed activity and sediment transport (Depth of Transport; *DoT*). Observations of *DoC* correspond closely to the values predicted by existing formulations based on inshore wave conditions (10–15 m for the study area; relative to mean low water spring water level in this case). The computed *DoT*, represented by the upper-plane bed transition attained under extreme conditions, exceeds 30 m depth in the study area. The significant implication is that, even though many headlands appear sufficiently prominent to suggest a closed boundary between adjacent embayments, significant wave- and tide-driven sediment transport is likely to occur beyond the headland base during extreme events, especially at low water levels. The maximum depth for significant sediment transport (*DoT*) was computed across a broad wave-current parameter space, further highlighting that tidal currents can increase this closure depth estimate by ~10 m along macrotidal coastlines, representing a 30% increase compared to tideless settings. This work illustrates the importance of tidal currents in depth of closure calculations and challenges the notion that embayed beaches are generally closed cells, as headland bypassing may be more wide spread than commonly assumed along exposed coastlines globally.

1. Introduction

Delineation of the active shoreface has long been a subject of investigation for coastal scientists and engineers (Hallermeier, 1978; Birkemeier, 1985; Wright et al., 1991; Wright, 1995; Ortiz and Ashton, 2016). The processes leading to sediment exchange across the shoreface, and the estimation of the seaward extent (depth) of those processes, are relevant to a wide range of coastal topics, including evaluation of sediment budgets (Hands and Allison, 1991; Capobianco et al., 2002), investigation of shoreface morphodynamics (Tanaka and Van To, 1995; Ortiz and Ashton, 2016), identification of the active zone for beach nourishment design (Hinton and Nicholls, 1998; Phillips and Williams, 2007; Aragones et al., 2016), computation of the long-term stability of beaches (Stive et al., 1992; Marsh et al., 1998), modelling coastal evolution (Hanson and Kraus, 1989; Larson and Kraus, 1992) and assessing the impact of sea-level rise on coasts (Stive et al., 1991; Rosati et al., 2013). Recognising the importance of appropriately framing the shoreface extent affected by intense bed activity, this offshore limit, denoted as 'depth of closure', remains a contentious subject in coastal science (Stive et al., 1991; Stive and de Vriend, 1995; Hinton and Nicholls, 1998; Nicholls et al., 1998b; Robertson et al., 2008; Ortiz and Ashton, 2016). Despite the availability of relatively robust nearshore sediment transport models, driven by appropriate hydrodynamic forcing (waves and tides), the concept also remains relevant, especially where resources to develop such numerical models are not available, for example due to lack of reliable bathymetric data.

* Corresponding author at: Reynolds Building, Drake Circus, Plymouth, Devon PL4 8AA, UK.
E-mail address: nieves.garciavaliente@plymouth.ac.uk (N.G. Valiente).

https://doi.org/10.1016/j.margeo.2018.10.009
Received 18 June 2018; Received in revised form 17 October 2018; Accepted 22 October 2018
Available online 24 October 2018
0025-3227/

The term 'depth of closure', hereafter *DoC*, is a theoretical concept used to limit two zones of different morphodynamic activity along the beach profile at short- and medium-term time scales (1–10 years): the *upper* shoreface is described as the area where significant changes on the beach profile are detected, while the *lower* shoreface is the area extending from the limit of significant change to the wave base where morphological change is negligible (or within the uncertainty limits), but intense bed agitation may occur under energetic wave conditions. The transition between the upper and lower shoreface is known as the morphological depth of closure (*DoC*) and the seaward extent of the lower shoreface is referred to as the maximum depth of significant sediment transport (*DoT*). Hence, *DoC* represents a morphodynamic boundary separating a landward, morphodynamically active region (Hallermeier, 1981; Hinton and Nicholls, 1998; Nicholls et al., 1998b), from a seaward region that is generally considered morphodynamically non-active. Of course, the definition of 'significant change' is ambiguous and depends on the time scale of consideration and the methods of morphological change detection; thus, different closure criteria may be used to define the corresponding closure points.

Embayed beaches are often considered closed systems, but even bounding headlands that appear sufficiently prominent to restrict headland bypassing under modal conditions, can 'leak' under extreme storms. Estimating the limit of the active shoreface under storm conditions in front of headlands allows identifying whether related embayments are open or closed sediment cells. Additionally, strong tidal currents associated with macrotidal settings are expected to move the closure limit of the active shoreface seaward. Therefore, where geological controls and strong tidal currents influence shoreface configurations, a re-evaluation of the 'active' nearshore limit seems appropriate. Here, we use the embayed, macrotidal and high-energy coasts of north Devon and Cornwall (UK) as a natural field laboratory to identify this limit using a multicriteria approach that includes: (1) observations of shoreface topography and sedimentology; (2) classic wave-based *DoC* parameterisations; and (3) bed shear stress computations. We focus on the investigation of the role of headlands in influencing *DoC* and *DoT*, and thus the potential for headland bypassing, thereby improving our understanding of shoreface dynamics on wave- and tide-dominated coasts.

The outline of this paper is as follows. Section 2 contextualizes the depth of closure concept and methods for its estimation employed to date. Section 3 presents a regional description of the North coast of Cornwall and Devon, as well as the prevailing dynamics affecting shoreface configuration along the coast. In Section 4, we present the methods for a multicriteria approach used to estimate *DoC* based on observations (Section 4.3.1), previously established wave-based parameterisations (Section 4.3.2) and modelling of wave- and current-induced bed shear stress (Section 4.3.3). In Section 5, results from the different approaches are explored. A discussion of the replicability and application of the different approaches for geologically-constrained and macrotidal coastal areas is presented in Section 6, followed by the conclusions of this research in Section 7.

2. Background

Several approaches have been pursued over the past four decades to estimate the morphological depth of closure. These can be synthesized in: (1) direct methods based on observations of morphological data (Hinton and Nicholls, 1998; Kraus et al., 1998; Nicholls et al., 1998b; Hartman and Kennedy, 2016); and (2) indirect methods that predict this depth based on wave hydrodynamics (Hallermeier, 1978, 1981; Roy and Thom, 1981; Birkemeier, 1985; Capobianco et al., 1997; Peters and Loss, 2012). Direct estimations are based on morphological data defining an envelope of variation that decreases with depth (Hinton and Nicholls, 1998; Kraus et al., 1998; Nicholls et al., 1998b; Hartman and Kennedy, 2016). Historically, *DoC* has been estimated using profile comparison as it is the most reliable method to estimate the point beyond which no significant changes on the profile are detected, where 'significant' generally relates to bed-level change larger than the detection limit. This traditional method requires an extended dataset (collected over several years at least) with repeated surveys along cross-shore transects of the beach, which ultimately makes it time-consuming and relatively expensive to obtain; therefore, direct estimates of *DoC* are only available from a small number of sites.

The challenge in accurately quantifying *DoC* motivated the development of indirect methods of prediction based on wave hydrodynamics and sediment characteristics affecting the shoreface. Examples of such indirect methods include wave-based formulations (Hallermeier, 1978, 1981; Birkemeier, 1985; Capobianco et al., 1997), energetics-based sediment transport methods (Ortiz and Ashton, 2016) and identification based on observations of sedimentary sequences (Roy and Thom, 1981; Nichols, 1999; Peters and Loss, 2012), as well as of abrupt changes in the textural composition of the seabed (e.g., Potter, 1967; Chesher et al., 1981; Larson, 1991; Work and Dean, 1991; Thieler et al., 2001).

Sedimentological approaches quantify the transition limit of areas with different wave activity as a particular change in the vertical stratigraphic sequence (sedimentary structures and bedforms); for example, hummocky stratification develops below normal fair-weather wave base during conditions analogous to the transition to upper plane-bed in unidirectional flow (Dott and Bourgeois, 1982). Studies of seabed composition often identify clear variations in texture and/or abrupt differences in sediment size along a beach profile (Potter, 1967; Chesher et al., 1981; Larson, 1991; Work and Dean, 1991). Sedimentological changes are more a reflection of the maximum depth of sediment transport (*DoT*) as both bedforms and sediment texture respond to wave-stirring and tidal current forcing, and they are not necessarily associated with morphological change as delimited by *DoC*.

Wave-based formulations propose different expressions to quantify limits of shoreface activity under the assumption that only the most energetic (i.e., largest) waves cause morphological change out to the closure depth (Hallermeier, 1981; Birkemeier, 1985; Capobianco et al., 1997). Hallermeier (1978, 1981) developed the first empirical approach to estimate the annual depth of closure (*DoC*) and maximum depth of bed activity (*DoC-motion*) on microtidal sandy beaches, based on the activity experienced by the seabed using laboratory experiments. According to these early studies, *DoC* represents the 'depth of significant morphological change', and is estimated as:

$$DoC = 2.28\, H_{12,t} - 68.5\left(\frac{H_{12,t}^2}{gT_t^2}\right) \tag{1}$$

where *DoC* is the predicted depth of closure over t years referenced to Mean Low Water (Hinton and Nicholls, 1998), $H_{12,t}$ is the non-breaking significant wave height that is exceeded for *12* h per t years, T_t is the associated wave period and g is the acceleration due to gravity. *DoC-motion* (Hallermeier, 1981) represents the limit for sediment motion and follows the expression:

$$DoC - motion = (\overline{H_{s,t}} - 0.3SD_s)\,\overline{T_{s,t}}\left(\frac{g}{5000D_{50}}\right)^{0.5} \tag{2}$$

where $\overline{H_{s,t}}$ is the annual mean significant wave height, SD_s and $\overline{T_{s,t}}$ are the associated standard deviation and average period of the significant wave height, respectively, and D_{50} is the median grain size.

Later, Birkemeier (1985), found that the expression for *DoC* (Eq. (1)) proposed by Hallermeier (1978) over-predicted observations by about 25% (Nicholls et al., 1998a) and proposed an adjusted expression for *DoC* of the form:

$$DoC = 1.75\, H_{12,t} - 57.9\left(\frac{H_{12,t}^2}{gT_t^2}\right) \tag{3}$$

Other authors proposed alternative formulations, simplifying the expression proposed by Hallermeier (1978). As an example, Capobianco et al. (1997), suggested an expression for *DoC*, which is

only a function of the non-breaking significant wave height exceeded for *12* h:

$$DoC = KH_{12,t}^{0.67} \quad (4)$$

where the constant K has value 3.4, 2.8 and 2.1 for a maximum vertical variation in the profile of 0.05, 0.1 and 0.2 m, respectively, over annual to medium temporal scale.

Eqs. (1), (3) and (4) have been shown to provide good predictions of the depth of closure on relatively-exposed, microtidal, sandy coasts. Nicholls et al. (1998a, 1998b) compared 12 years of bathymetric data and nearshore wave statistics from Duck, NC. They showed that Eq. (1) provided conservative estimates of the annual depth of closure values for different closure criteria (maximum vertical variation of 0.06 m, 0.1 m, and 0.15 m), but successfully predicted the closure limit (*DoC*) during erosional events. Later, Robertson et al. (2008) tested Eqs. (2) and (4) using observations of measured changes in the peninsula of Florida and showed that Hallermeier's (1978) wave-based formulation best matched the observations of that area. In all mentioned studies, these formulations were tested on a microtidal coast and they may not necessarily be directly transferable to macrotidal beaches (Nicholls et al., 1998a). According to Hallermeier (1978), the effect of tidal action on Eq. (1) can be accounted for by referencing the depths obtained relative to mean low water (MLW), but this only provides a tidal datum adjustment and does not account for the role of tidal currents.

Although wave-based formulations continue to be a common and widely-accepted approach to predict *DoC*, other approaches are appearing in the literature. Robertson et al. (2008) presented the influence of non-erodible beds or hardgrounds on *DoC* using airborne bathymetric data, and suggested that this method based on observations is a good approach to follow in areas where the presence of bedrock plays an important role in determining the depth of closure. In addition to the mentioned geological control, other authors have also pointed out to a clear influence of the tidal currents in the estimation of *DoC* (Hartman and Kennedy, 2016). Following these more recent suggestions, the usefulness of the wave-based formulations is evaluated here along an area where geological control (presence of bedrock and headlands as attenuation and refraction points), large tidal ranges and strong tidal currents are essential components in explaining sediment dynamics on the shoreface. This provides a novel and updated evaluation of the depth of closure concept emphasizing the role of these in predicting the zone of active sediment transport.

3. Study area

The North coast of Cornwall and Devon, Southwest England (UK), extends 200 km from Land's End (SW) to Ilfracombe (NE) (Fig. 1). The coastline comprises high and hard rock cliffs (up to 120 m above sea level), rocky headlands, small estuaries and relatively short sandy embayed beaches (< 5 km), spanning reflective to dissipative conditions (Scott et al., 2011), often backed by dune systems and/or cliffs. The configuration of the shoreface is highly variable (Scott et al., 2011) and includes: (1) large and deep bays with multiple beaches/embayments of varying west to north orientation; (2) steep and narrow shorefaces with shallow and mainly west-facing embayments separated by headlands; and (3) rocky cliffs fronted by sandy beaches, without clear embayments. The average grain size for this coast is 0.3 mm (Prodger et al., 2016). This coast receives a combination of Atlantic swell, primarily from the west to WNW, and local wind waves. A wave height gradient exists from SW to NE (Fig. 1, top panel), with mean significant wave height (H_s) decreasing from 1.9 m at Land's End (SW) to 1.0 m in Ilfracombe (NE), with associated peak periods (T_p) of 9.8 s and 11.0 s, respectively. The coastline is macrotidal: the largest tides are experienced in the Bristol Channel where the mean spring tidal range (MSR) is 8 m and the smallest tides in the region occur at Land's End (MSR = 5 m).

Along most of the coast, the maximum ebb and flood velocity ranges from 0.1 to 0.4 ms^{-1} at depths between 10 and 30 m (Fig. 2) with the tidal flows predominantly parallel to the shoreline. The strong flood-ebb asymmetry in the current magnitude during a tidal cycle results in a northward tidal net flux along the coast. At depths exceeding 30 m, the maximum tidal current ranges from 0.3 ms^{-1} to 0.6 ms^{-1} in front of the embayments, and significantly increases around the headlands (Fig. 2, right panels), where maximum tidal flows can be of the order of 1 ms^{-1} (*Region 1* at 30 m depth; Fig. 2, bottom right panel) and even exceed 1.2 ms^{-1} in locations close to the Bristol Channel (e.g., in *Region 6* at 30 m depth; Fig. 2, upper right panel). Strong tidal velocities are also observed around headlands in central regions (*Region 3–5*) with values of flood current higher than 0.4 ms^{-1} at 20–30 m depth (Fig. 2, middle right panel).

For the analysis, the coastline was divided into six regions (Fig. 1, bottom panel) based on geomorphic and hydrodynamic characteristics (Table 1), and includes 25 individual low tide embayments (LTEs), which are defined as embayed systems that represent a single embayment at low tide, but may be split up into smaller beaches at high tide. *Region 1* (Fig. 3a) represents the southernmost area and covers Whitesand Bay, a concave calcareous-sandy wide bay disrupted by a rocky section at 20 m water depth. This region contains the steep and narrow beaches of Sennen Cove and Gwenver (Fig. 3g). *Region 2* covers St. Ives Bay (Fig. 3b), a shallow crescentic bay with a wide and flat shoreface (Fig. 3g). Three LTEs are present (Porthmeor, Carbis Bay and Godrevy) with sand present up to 25 m depth. *Region 3*, from Porthtowan to Fistral, is characterized by wide dissipative sandy beaches embayed by prominent headlands, backed by large dunes and alternating with stretches of rocky sediment-free areas with 50–90 m high cliffs. Six LTEs (including Perranporth, Fig. 3c) with steep to moderate shorefaces are present here. *Region 4*, from Newquay to Polzeath, is a relatively straight and exposed section of coast, with a sandy layer covering a partially exposed rock platform with headlands acting as constraining points, and with cliffs with heights of 40–60 m. Two types of LTEs are present in *Region 4*: the first group (Newquay Beaches, Fig. 3d) are crescentic sandy bays, while the second group (Bedruthan Steps, Treyarnon) are narrower (Fig. 3g), coarser, more exposed and straighter. *Region 5* is relatively straight and embayments are notably absent (Fig. 3e). This coastline is characterized by narrow and long patches of coarse sand (to −20 m Ordnance Datum Newlyn, ODN; Fig. 3g) constrained by small headlands and a landward cliff. *Region 6*, from Westward Ho! to Woolacombe, is the northern-most region, with sandy beaches embayed by cliffed rocky headlands (Fig. 3f). Sediment is finer and the shoreface slope is shallower (Fig. 3g) than in the other regions, with sand to −30 m ODN, and with an average distance from the 0 isobath to −30 m ODN of 3600 m for Woolacombe and > 8000 m for Westward Ho!, Saunton and Croyde.

4. Methodology

Our approach is to compare several criteria for determining the 'active' nearshore limits and these are grouped under three methods (Fig. 4): $DoC_{obs,a–c}$ is based on observations, $DoC_{param,a–b}$ uses wave-based formulations and $DoC_{stress,a–b}$ uses numerical modelling outputs.

4.1. Observational data

A 10-year time series of beach morphology and subtidal bathymetry of Perranporth beach (*Region 3*, Fig. 3c) was used to determine observed depth of closure ($DoC_{obs,a}$, Fig. 4). Field data were collected using RTK-GPS for the supra- and intertidal beach and single-beam echo-sounder for the subtidal area . The uncertainty limit for detecting significant morphologic change was $\Delta d \leq 0.14$ m (± 0.14 m corresponds to the uncertainty associated with the field data collection; RTK-GPS input into Valeport MIDAS Surveyor is accurate to ± 0.02%). Data were merged and interpolated using the quadratic loess method (Plant et al.,

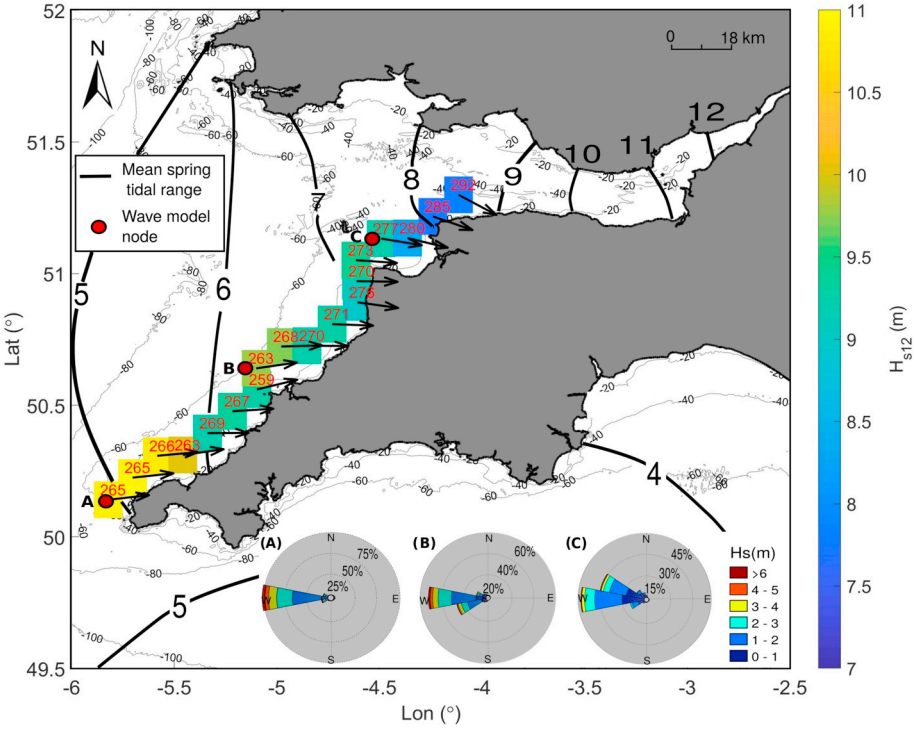

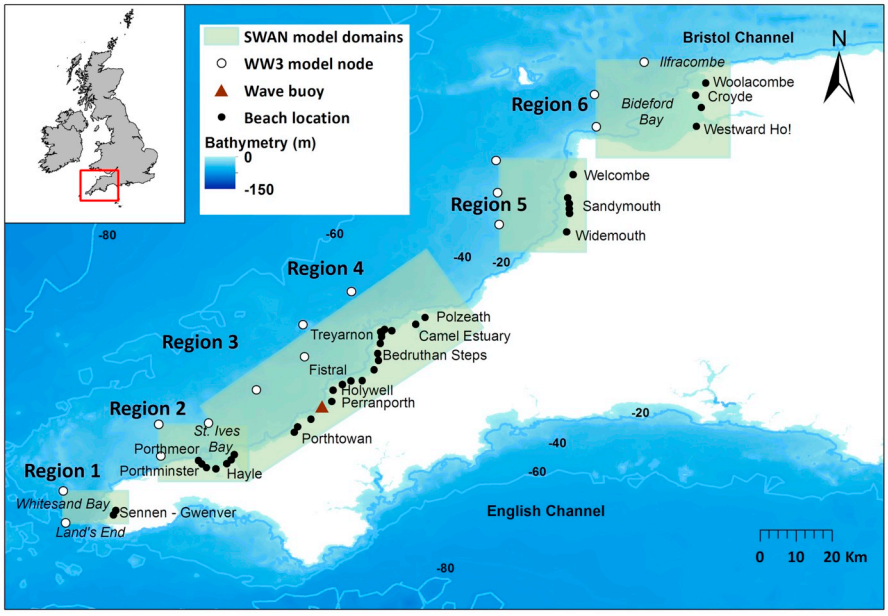

Fig. 1. Study area, SW England. Top panel: wave climate variability and tidal range. Wave climate data represent a 4-year record (2013–2016) from the MetOffice WW3 model, with cell colour indicating offshore H_s exceeded 12 h per year and associated direction. Red circles (A to C) indicate the locations of wave roses. Black solid lines represent mean spring tidal range, adapted from BERR (2008). Bottom panel: location of study areas along the SW (SWAN model domains for *Regions 1–6*). Black dots indicate the studied embayments and white circles are MetOffice UK Waters Wave Model nodes used as SWAN input. (For interpretation of the references to colour in this figure legend, the reader is referred to the web version of this article.)

2002) to produce DEMs, providing a time series sufficiently long to compare observed closure depth with that predicted using wave-based theoretical methods. Complementing the morphological dataset, sediment size distribution ($DoC_{obs,b}$, Fig. 4) along Perranporth shoreface (from +4 to −30 m) was analysed using sediment samples collected during winter and summer 2016 (Samuel, 2017).

Regional LiDAR (provided by Plymouth Coastal Observatory) and multi-beam bathymetry (United Kingdom Hydrographic Office, 2011) were used to conduct a comparison of shoreface characteristics across the six regions and to determine the sand-rock transition depth of closure ($DoC_{obs,c}$, Fig. 4). A digital elevation model (DEM) was constructed for the coast of SW England by combining the LiDAR (up to −3 m) and multi-beam bathymetry (to < −50 m), corrected and referenced to Ordnance Datum Newlyn (ODN) using the Vertical Offshore Reference Frame model (VORF) made available by the United Kingdom Hydrographic Office.

4.2. Numerical modelling data

4.2.1. Wave models (WW3 and SWAN)

Wave statistics are required to calculate parameterised estimates of depth of closure (Section 4.3.2, DoC_{param}) and shear stress (Section 4.3.3, DoC_{stress}). Hindcast wave conditions were obtained from the MetOffice UK Waters WaveWatch III (WW3) Model (Tolman, 2014; Saulter, 2017) for 18 nodes at 8-km resolution across *Regions 1–6* (cells in Fig. 1, upper panel) over a 4-year period (01/01/2013–01/01/2016). This includes the winter of 2013/14, ranked as the most energetic winter under the last seven decades (Masselink et al., 2015).

Offshore wave conditions (at > 50 m depth, white circles in Fig. 1, bottom panel) may not be representative of inshore conditions (at

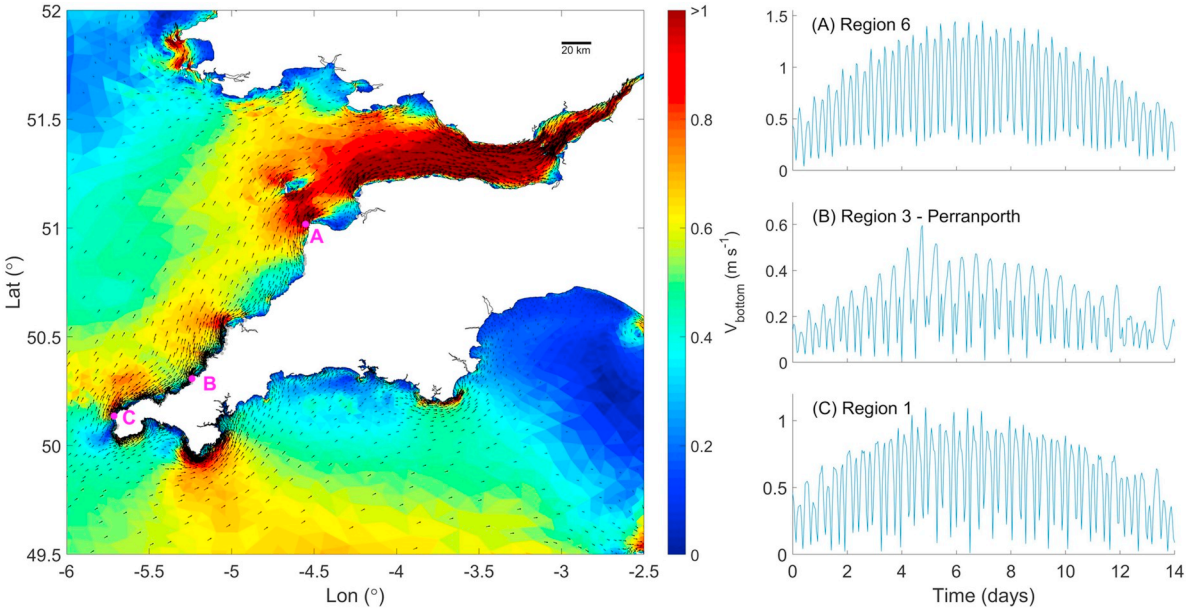

Fig. 2. Left panel: Spatial distribution of bottom tidal current velocities and direction during spring tides. Magenta dots with labels (A, B, C) represent locations of velocity time series shown in the right panels. Right panels: velocity current time series for a neap-spring-neap tidal cycle at the 30-m contour line off the headlands for *Region 6* (upper), Perranporth-*Region* 3 (middle) and *Region 1* (lower). Data sourced from FVCOM numerical model (Chen et al., 2003), produced by the UK National Oceanography Centre. (For interpretation of the references to colour in this figure legend, the reader is referred to the web version of this article.)

Table 1
Deep-water wave climate statistics for the selected regions using hourly wave model outputs from the MetOffice UK Waters Wave Model, 2013 to 2016.

Region	Hydrodynamics						Morphology		
	H_s (m)	$H_{s99\%}$ (m)	H_{s12} (m)	T_p (s)	$T_{p99\%}$ (s)	T_{p12} (s)	D_{50} (mm)	Slope	Orientation
1	1.9	7.0	10.0	9.8	16.4	18.2	0.49	0.028	NW-W
2	1.7	6.7	9.5	9.8	16.4	18.2	0.37	0.008	NNE-WNW
3	1.6	6.1	9.3	10.2	16.7	18.2	0.37	0.013–0.021	W-NW
4	1.6	5.8	8.8	10.1	16.4	17.9	0.34	0.013	W-NW
5	1.5	5.8	8.4	10.9	17.0	18.5	0.48	0.017	W
6	1.4	5.1	7.3	11.0	16.7	18.5	0.33	0.005	W

H_s – significant wave height; $H_{s99\%}$ – 99th percentile; H_{s12} – significant wave height exceeded 12 h per year; T_p – peak period.

15–20 m depth) within deep embayments and/or on coastlines that do not face into the prevailing wave direction; therefore, the *DoC* computed using offshore conditions may not be appropriate. Accordingly, the third-generation spectral wave model SWAN (Booij et al., 1999) was used to transform wave conditions from offshore to inshore. This model accounts for wind growth, dissipation processes and wave-wave interactions. SWAN was set up for five domains (one for each region, except regions 3 and 4 which had a shared domain; Fig. 1, bottom panel) using a rectangular grid with a resolution of 100 × 100 m. The dissipation mechanisms considered were bottom friction (with JONSWAP friction coefficient of 0.067 $m^2 s^{-2}$), refraction, whitecapping (Komen et al., 1984) and depth-induced breaking (with ratio of maximum individual wave height over depth equals to 0.73). Non-linear wave-wave interactions were also considered (TRIADS mechanism). SWAN output was validated against wave height observations (wave buoy in Fig. 1, bottom panel) for February 2014 and the model satisfactorily reproduced wave height, period and direction. Wave height is well predicted and showed a bias of only −0.06 m and a root-mean square error (RMSE) of 0.003 m. Peak period prediction is excellent (bias = −0.05 s; RMSE = 0.02 s).

4.2.2. Tide and surge model (FVCOM)

Data from the finite-volume, three-dimensional (3D) hydrodynamic model FVCOM (Chen et al., 2003) provided by the National Oceanography Centre were used to compute current bed shear stress (Section 4.3.2, DoC_{stress}). The FVCOM domain covers the NW European shelf and the horizontal spatial resolution of the space-varying unstructured cells of the model grid ranges from 2 km offshore to 100 m near the coast. A σ layer (terrain following) coordinate system of 10 uniform layers was used for vertical discretization. Model validation results against tide gauge (Ilfracombe and Newlyn) for total water elevation showed a bias of −0.002 m and a RMSE of 0.26 m. Current meter data collected in 20-m water depth off Perranporth (Region 3, Fig. 2c) were also compared with FVCOM model data. Recorded maximum current speeds during spring tides at this location were 0.4 ms^{-1} and were well reproduced by the numerical model (0.42 ms^{-1}; bias = 0.09 ms^{-1}). FVCOM was run for the year 2008 including full meteorological forcing (tidal, river, surface heat, surface wind and surface precipitation forcings). Hourly data of water surface elevation and eastward/northward flow velocity along the SW shelf of England for March 2008 were extracted from the model results. The period used for the hydrodynamic model (2008 in this case) does not represent major implications in our depth of closure computations as the hydrodynamic model output was only used to obtain tidal current velocities for a representative tidal cycle during spring tides. For a detailed description of a similar FVCOM model set-up and parameterisation refer to De Dominicis et al. (2017).

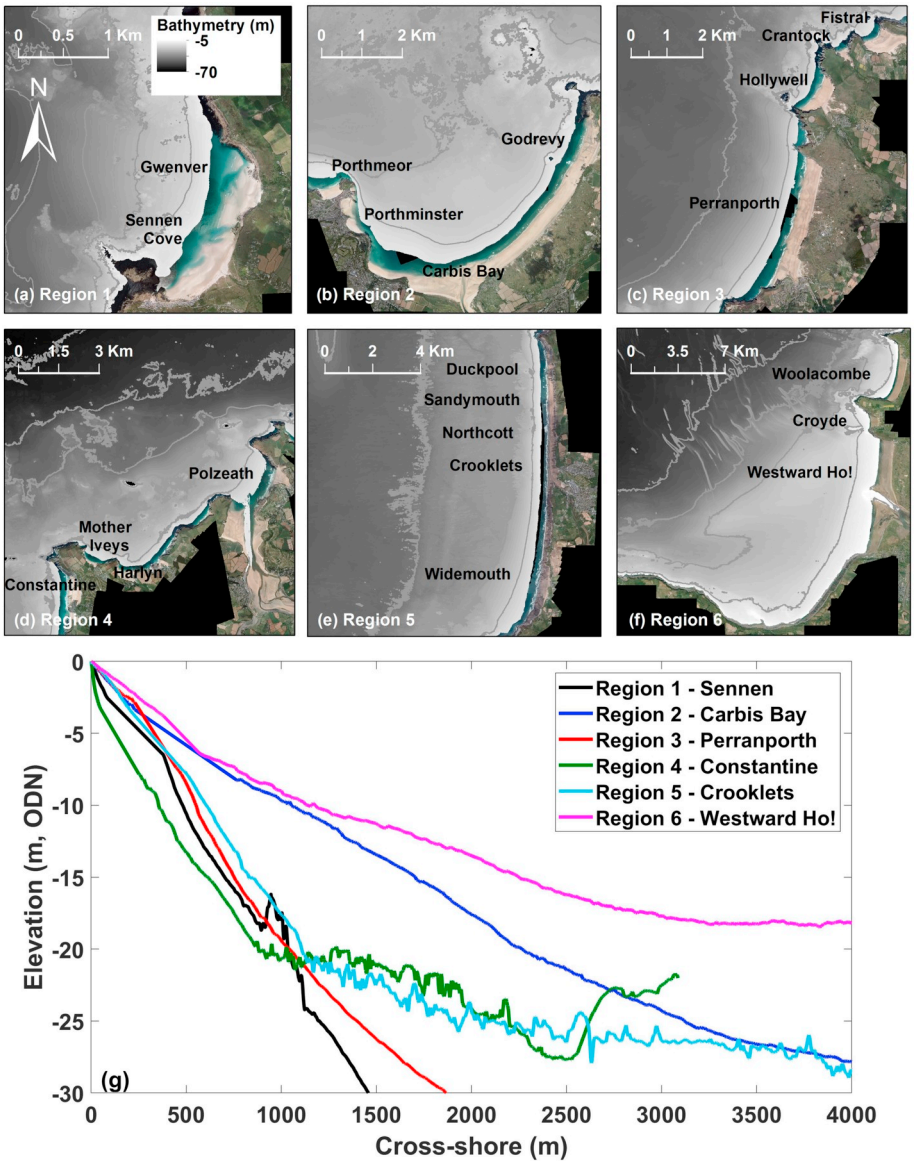

Fig. 3. Upper panel (a–f): aerial photography and bathymetry for the six regions of study. Lower panel (g): representative shoreface profiles extracted from the central part of selected LTEs. Bathymetry data were obtained from United Kingdom Hydrographic Office (2011) and aerial photographs were courtesy of Plymouth Coastal Observatory (available at https://www.channelcoast.org/southwest/). (For interpretation of the references to colour in this figure legend, the reader is referred to the web version of this article.)

4.3. Depth of closure methods

4.3.1. Observed depth of closure (DoC_{obs})

Direct field observations included calculation of the envelope of morphological change ($DoC_{obs,a}$), sediment size distribution ($DoC_{obs,b}$) and sand-rock transition ($DoC_{obs,c}$). Direct morphological change observations and sediment size distribution for one of the study sites (Perranporth, *Region 3*) were used to test the applicability of the parametric wave-based formulations (DoC_{param}) and the proposed process-based method (DoC_{stress}). The seabed sediment observational dataset was also compared with the presence of sediment (sand-rock transition) in 164 representative cross-shore profiles (covering 25 low tide embayments, LTEs) that were extracted along the six regions.

The Perranporth 10-year time series DEMs (Section 4.1) were alongshore-averaged across a 250-m section (black box on Fig. 5, right panel) to enable the identification of the point at which morphological change can be considered insignificant ($\Delta d \leq 0.14$ m; $DoC_{obs,a}$). The observed depth of closure at Perranporth was supplemented by a grain size analysis ($DoC_{obs,b}$) at one representative cross-shore profile. Sediment samples corresponded to winter and summer conditions (March and July 2016), providing a seabed sediment distribution representative of high energy conditions. Depths at which grain size significantly changed were identified (e.g., sand to gravel).

The final observational method for determining depth of closure was to identify the sand-rock transition ($DoC_{obs,c}$) using a regional DEM constructed from LiDAR and multi-beam data (Section 4.1). The regional DEM of the SW England was used to compare the shoreface profiles across *Regions 1–6*. A total of 164 profiles were extracted (up to −30 m ODN), representative of the different study sites. The transition point between sand and rock was manually identified based on a change from smooth to rough bed and/or a break in the shape of the shoreface profiles (e.g., Fig. 3g, *Region 1* at 800 m offshore).

4.3.2. Wave-based formulations (DoC_{param})

The empirically determined wave-based formulations (DoC_{param}) based on significant wave height and peak period for a given region

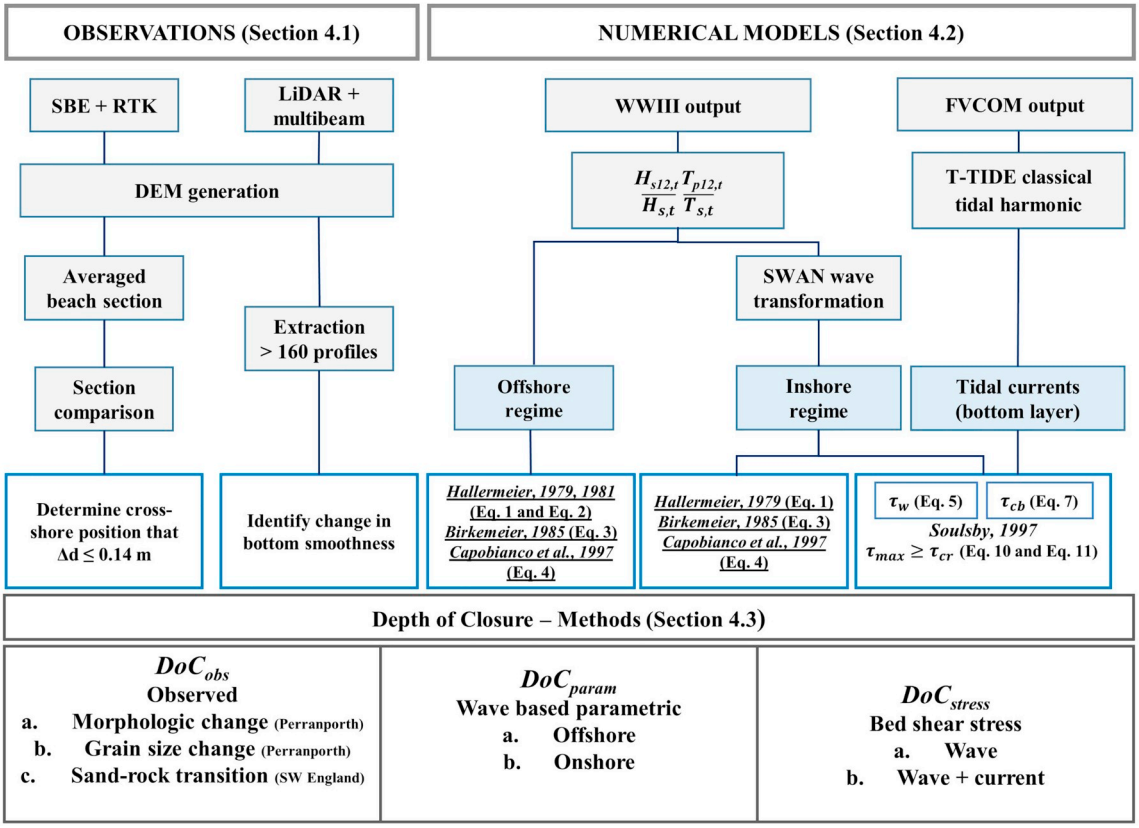

Fig. 4. Flow diagram of research methodology of the *DoC* quantification. Underlined criteria correspond with the methods to test.

were described in Section 2 (Eqs. (1)–(4)). First, the offshore wave conditions were used to compute at each WW3 node (Fig. 1, bottom panel) the depth of closure parameters ($DoC_{param,a}$), specifically *DoC* (Eqs. (1), (3), (4)) and *DoC-motion* (Eq. (2)), and then averaging across all nodes in each of the six regions. *DoC-motion* was computed using the median grain size typical from the SW (0.3 mm) for the total time series ($t = 4$ years), while *DoC* was calculated for both the total 4-year time series, as well as independently for each individual year ($t = 1$ year) and then averaged $\langle DoC \rangle$. For clarity, when *DoC* is used without chevrons, it is averaged over the full extent of the available data, while $\langle DoC \rangle$ with chevrons indicates averaging the 1-year results over the 4-year period.

Parameterising depth of closure values for the inshore region ($DoC_{param,b}$) requires wave transformation using SWAN (Section 4.2.1).

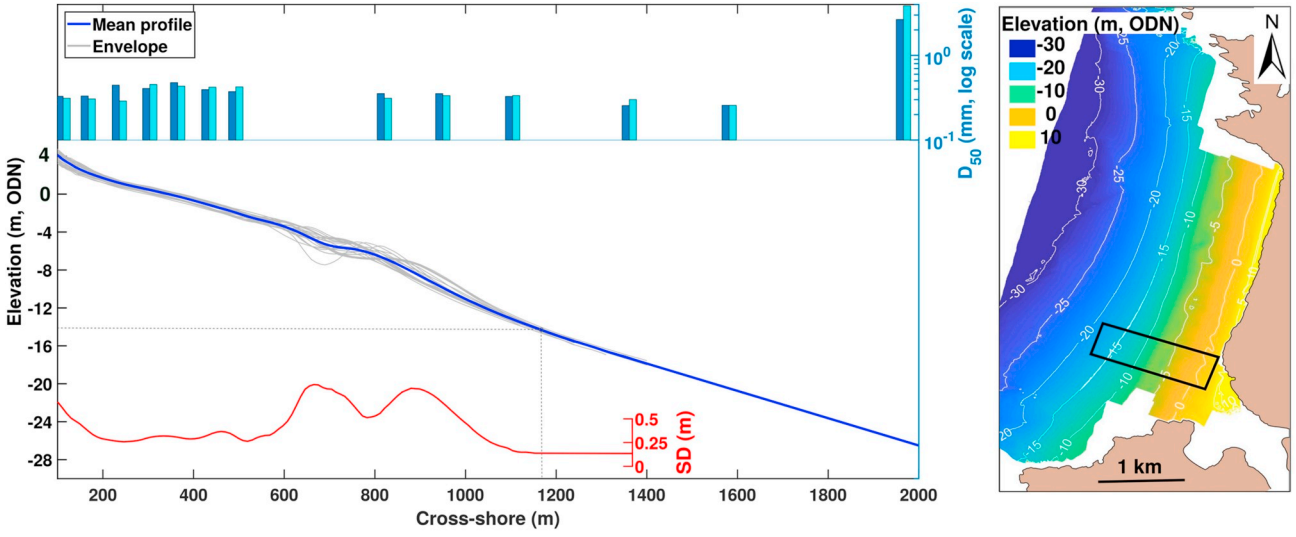

Fig. 5. Left panel: observed depth of closure estimated for Perranporth beach, north Cornwall, from the profile envelope ($DoC_{obs,a}$) and from sediment distribution ($DoC_{obs,b}$). Light and dark blue bars represent the median sediment size (D_{50}) for winter and summer samples, respectively. The grey lines represent alongshore-average profiles associated with beach survey data collected from 2010 to 2016; the blue line is the mean profile over the survey period; and the red line shows the standard deviation associated with the mean profile. The dashed line represents *DoC* based on the morphological observations. Right panel: topographic and bathymetric survey with 250-m wide section of beach (black box) for alongshore-average profile used in left panel. (For interpretation of the references to colour in this figure legend, the reader is referred to the web version of this article.)

The sediment motion depth of closure *DoC-motion* as described by Hallermeier (1981) is not presented for inshore locations, as this depth is commonly located beyond the rocky headlands and falls beyond the regional model domains. Spatially-varying inshore values for the morphological depth of closure were determined as follows: (i) for each of the six regions, the offshore modelled wave data were ordered into seven 30°-directional bins with bin centres from 180° to 360°; (ii) for each of these classes, the wave heights were ranked, and the significant wave height exceeded for 12 h ($H_{s12,t}$) and associated peak period ($T_{p12,t}$) were computed for $t = 4$ years and $t = 1$ year; (iii) SWAN models were run for each region using these extreme wave values; (iv) an iterative method (refer to Kraus et al., 1998) was used to extract inshore wave height and associated period at the actual predicted *DoC* and ⟨*DoC*⟩ across each domain, using Eqs. (1), (3) and (4); (v) a representative *DoC* and ⟨*DoC*⟩ value was obtained for each embayment by alongshore-averaging; and (vi) the depth of closure was calculated relative to MLWS, then corrected to the survey datum (ODN).

4.3.3. Bed shear stress (DoC_{stress})

The approach for estimating the limit of significant sediment transport (*DoT*) under storm conditions and on a macrotidal regime was through analysis of numerically-modelled bed shear stress induced by waves (τ_w) and tidal currents (τ_{cb}), referred to as methods $DoC_{stress,a}$ and $DoC_{stress,b}$, respectively (refer to Fig. 4). Bed shear stress was computed following Soulsby (1997) and compared with different thresholds of initiation of motion and bedform activity according to Nielsen (1981).

The bed shear stress produced by waves is generally the main forcing control on sediment transport in shallow water (< 30 m depth) in exposed (wave-dominated) coastlines. The wave-induced shear stress was computed for the six regions (five SWAN wave model domains) for the extreme wave values (H_{s12}, T_{p12}). Wave bed shear stress is oscillatory and was obtained using:

$$\tau_w = \frac{1}{2}\rho f_w U_w^2 \tag{5}$$

where f_w is the wave friction factor, $U_w = \sqrt{2}\,U_{rms}$, and U_{rms} is the root-mean-square wave orbital velocity near the bed. According to Soulsby (1997), the wave friction factor for turbulent flow depends on the bottom roughness parameter ($z_0 = D_{50}/12$) and the semi-orbital excursion ($A = U_w T/2\pi$) as follows:

$$f_w = 1.39\left(\frac{A}{z_0}\right)^{-0.52} \tag{6}$$

Tidal current bed shear stress was determined using classical tidal harmonic analysis on FVCOM current outputs using T-TIDE (Pawlowicz et al., 2002) for the entire FVCOM domain and at each model node. Tidal currents were resolved using the eight major tidal constituents *S2*, *M2*, *N2*, *K2*, *K1*, *P1*, *O1* and *Q1*, and the shallow water constituents *O2*, *N4*, *M4* and *S4*. Current bed shear stress was then computed using only tidal forcing for one representative tidal cycle during spring tides following a quadratic drag law expressed as:

$$\tau_{cb} = \rho C_d \overline{U}_{cb}^2 \tag{7}$$

where τ_{cb} is the bottom (friction) stress induced by tidal currents, ρ is the water density, $\overline{U}_{cb}$ is the maximum near bottom depth-averaged flow velocity for a tidal cycle (during spring tides) in analogy to selecting the maximum wave forcing conditions, and the drag coefficient, C_d, is determined along the domain by matching a logarithmic bottom layer at a height z_{ab} above the bottom (see e.g., Young, 1999). Thus:

$$C_d = max\left[\frac{k^2}{ln\left(\frac{z_{ab}}{z_0}\right)^2}, 0.0025\right] \tag{8}$$

with k being the von Karman constant ($k = 0.4$) and z_0 is the bottom roughness parameter.

The combined wave and current bed shear stress τ_m cannot be obtained as a simple linear sum of the separate stresses due to the non-linear interaction between wave and current boundary layers. Soulsby (1995) found a good fit between the observations in the laboratory and a theoretical model based on a two-coefficient optimization of the form:

$$\tau_m = \tau_{cb}\left[1 + 1.2\left(\frac{\tau_w}{\tau_{cb} + \tau_w}\right)^{3.2}\right] \tag{9}$$

in which τ_{cb} and τ_w are the current- and wave-induced shear stresses respectively, computed individually. The corresponding expression for τ_{max} is given as follows:

$$\tau_{max} = [(\tau_m + \tau_w\,|\cos\varnothing|)^2 + (\tau_w\,\sin\varnothing)^2]^{1/2} \tag{10}$$

where ∅ is the angle between the direction of wave travel and the current component.

Soulsby (1997) related sediment motion threshold for a specific seabed with the critical Shields parameter θ_{cr} through the expression:

$$\tau_{cr} = \theta_{cr} g(\rho_s - \rho) D_{50} \tag{11}$$

where ρ_s is the sediment density and g is gravitational acceleration. This algorithm calculates critical shear stress (τ_{cr}) for non-cohesive and well-sorted particles using a non-dimensional Shield's curve. Critical shear stresses were calculated using the average grain size typical of SW England – $D_{50} = 0.3$ mm, as well as $D_{50} = 0.15$ and 0.6 mm. The use of the different sediment sizes allows analysis of the sensitivity of threshold exceedance of combined wave and current bed shear stress to seabed composition.

According to Eq. (11), initiation of motion, as well as sediment transport, will depend on boundary shear stresses and seabed characteristics. Based on laboratory experiments and observations, Nielsen (1981) determined that the occurrence of bedforms is related to the bed shear stress (τ or θ) and developed a relation between bedform type and wave energy conditions, expressed as a function of transport stage. Using Grant and Madsen (1982), the following critical values of the Shields number (θ_{cr}) can be identified: (i) initiation of motion $\theta_{cr} = 0.048$; (ii) formation of sharp-crested vortex ripples $\theta_{cr} = 0.1$; (iii) transformation from vortex to post-vortex ripples $\theta_{cr} = 0.2$; and (iv) transition into a plane bed $\theta_{cr} = 1$. Following Eq. (11), combined wave- and current-induced bed shear stress was computed for each region and compared with the critical shear stresses τ_{cr} for the different bedform scenarios.

5. Results

5.1. Closure depth based on observations: Perranporth case of study ($DoC_{obs,a\text{-}b}$)

Survey (beach and bathymetry) data from Perranporth, one of the west-facing embayments of *Region 3* (Fig. 1, bottom panel for location), was used to derive the observed closure depth for this location (*DoC*, $DoC_{obs,a}$). Fig. 5 shows the mean and the standard deviation (SD) associated with all alongshore-averaged shoreface profiles for Perranporth collected over the period 2010–2016. The largest bed-level variability (SD > 0.5 m) occurs in the outer bar region (x = 700–900 m). This vertical variability decreases offshore to < 0.14 m at a depth of 14.5 m (ODN), and this depth is considered the morphological depth of closure for this embayment as 0.14 m is the uncertainty associated with the survey data.

Several authors in the literature analyse textural changes in the seabed to determine the boundaries of the active profile (Potter, 1967; Chesher et al., 1981; Larson, 1991; Work and Dean, 1991). Following that approach ($DoC_{obs,b}$, refer to Fig. 4), sediment samples collected during winter and summer 2016 at 13 different locations on the shoreface profile are presented in Fig. 5. Supratidal D_{50} values are relatively constant with a value of 0.33 mm. The coarsest sediments in the

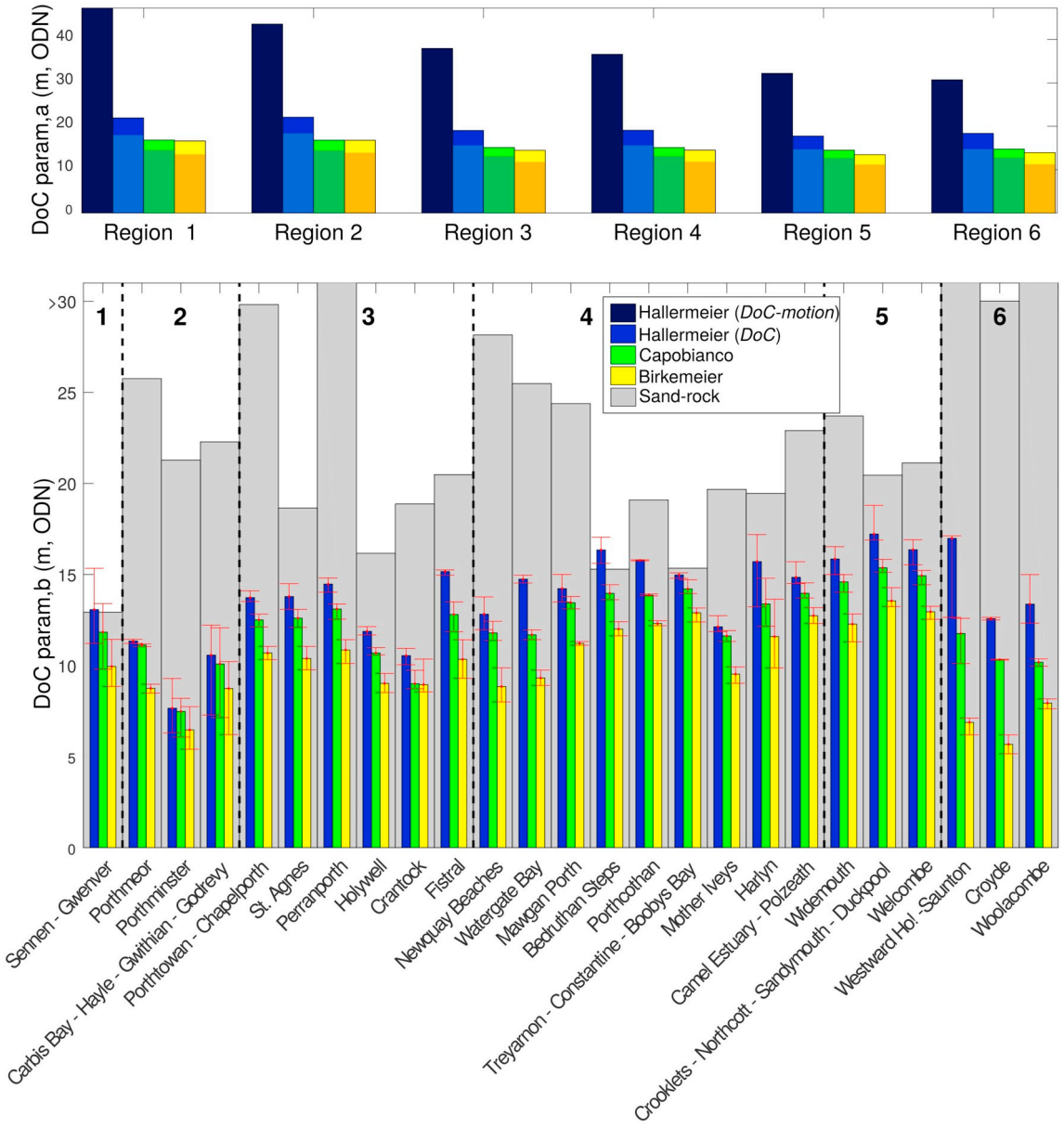

Fig. 6. Along-coast variability in depth of closure obtained by applying the wave-based formulations of Hallermeier for *DoC* (light blue) and *DoC-motion* (dark blue), Capobianco (green) and Birkemeier (yellow). Upper panel: *DoC* at each region computed using offshore WW3 wave conditions ($DoC_{param,a}$). Light bars show *DoC* values for $t = 4$ years and darkest colour bars represent *DoC* ($t = 1$ years). Bottom panel: bars represent the average *DoC* for each embayment, computed using the modelled inshore wave conditions and forcing the SWAN wave model with $H_{s,12}$ and $T_{p,12}$ derived from the 4-year time series ($DoC_{param,b}$). Minimum and maximum *DoC* values for each embayment are represented by the red intervals. Grey bars represent the embayment-averaged depth of the transition between sand and rock. Vertical black dashed lines separate the different regions. (For interpretation of the references to colour in this figure legend, the reader is referred to the web version of this article.)

upper part of the profile (0.48 mm) are found around the Mean Spring Low Tide level. Seaward of this point, sediment size decreases with depth from 0.40 mm at z = −3 m, 0.33 mm at z = −18 m and 0.30 mm between −22 m and −26 m. With increasing depth, D_{50} abruptly increases to 2.657 mm, representing a transition to gravel. This change in the sediment size is also observed in backscatter data (unpublished data), where the presence of medium sand along the embayment domain is interrupted by gravel patches around the −26 m contour line.

5.2. Along-coast variability in depth of closure (DoC_{param}, $DoC_{obs,c}$)

The different depth of closure measures computed using the various wave formulations DoC_{param} (Eqs. (1)–(4)) are summarized in Fig. 6. The sediment motion depth of closure determined using mean wave characteristics (*DoC-motion*, Eq. (2)) was calculated for each of the six regions (Fig. 6, upper panel) and decreases from 50 m in the south to 34 m in the north, in response to the associated decrease in wave energy (Fig. 1, top panel). The morphological depth of closure estimate was calculated over 4-years (*DoC*) and for 1-year averages (⟨*DoC*⟩) for three different formulations (Eqs. (1), (3) and (4)). *DoC* decreases from 23 m in the south (*Region 1*) to 19 m in the north (*Region 6*) for Hallermeier (1978), and the corresponding values for the Capobianco et al. (1997) and Birkemeier (1985) formulations are shallower, ranging from 17 m to 14 m, and from 15 to 12 m, respectively. The decrease in depth of closure over decreasing time scale is demonstrated through comparison with the ⟨*DoC*⟩ values (Fig. 6, top panel-darkest bars), which are 4 m, 2 m and 1.5 m less than those obtained using the total time series (*DoC*, Fig. 6, top panel-light bars) for Hallermeier (1978), Capobianco et al.

(1997) and Birkemeier (1985), respectively.

Embayment-averaged *DoC* results are obtained using wave conditions transformed to the nearshore ($DoC_{param,b}$) and, most significantly, there is no obvious correlation between the depth of closure values computed using the offshore (Fig. 6, top panel) and inshore (Fig. 6, bottom panel) wave formulations. While *DoC* computed from offshore wave conditions ($DoC_{param,a}$) *decreases* from south to north, the value computed using inshore wave conditions *increases* from *Region 1* to *Region 5*, then decreases for *Region 6*. This emphasizes the very significant role nearshore morphology and embayment orientation play in attenuating wave energy. Clearly, if untransformed wave values are used to estimate *DoC* for highly embayed coasts, the results are likely to be significantly overestimated. *DoC* values computed using inshore wave conditions using Hallermeier (1978) (Eq. (1)) are in all cases 1–2 m larger than results using Capobianco et al. (1997) (Eq. (4)) and Birkemeier (1985) (Eq. (3)). As an example of the results, typical values of *DoC* using Hallermeier (1978) ($DoC_{param,b}$) for the most exposed parts of the coast (*Regions 1*, *5* and *6*, and the north part of *Regions* 3 and *4*) are 12–16 m (relative to ODN), whereas *DoC* values for the more sheltered parts (*Regions 2* and the south part of *Region 6*) are typically 6–10 m.

The sand-rock transition depth ($DoC_{obs,c}$) is presented in Fig. 6 (bottom panel, grey bars) for comparison with the depth of closure estimates obtained using the wave formulations. There is no obvious alongshore correlation between the sand-rock transition and either the offshore or inshore wave formulations, and this is attributed to sediment availability being a more important factor in determining the sand-rock transition than the hydrodynamic forcing. Additionally, there are no clear alongshore trends in the sand-rock transition. The sand-rock transition ranges from 15 m to > 30 m water depth, which is generally significantly deeper than *DoC*, and in some instances double that of the computed *DoC* (e.g., Porthmeor, Perranporth, Widemouth, Woolacombe). One exception is Bedruthan Steps, where Eq. (1) predicts *DoC* at 16 m, while the rocky platform begins at 15 m depth, suggesting this embayment is particularly sediment-starved. At Sennen Cove, the sand and rocky platform transition and *DoC* (based on Eq. (1)) are at a similar depth. Significantly, these results suggest that the upper shoreface active profile for the SW generally has sufficient sediment (*DoC* < sand-rock transition). However, on the lower shoreface, where sediment transport is more infrequent, there tends to be a lack of available sediment (sand-rock transition < *DoC-motion*).

The occurrence of significant along-embayment variability in depth of closure using $DoC_{param,b}$ (Hallermeier, 1978) is exemplified in Fig. 7. Along-embayment variability occurs at locations that display a considerable difference in the shoreline orientation and, therefore, a spatial gradient in the wave conditions. This results in higher *DoC* values for more exposed sections (e.g., > 15 m for the W section, Fig. 7) compared to more sheltered section (e.g., 5–7 m for the NNE section, Fig. 7). Such large differences are particularly relevant in *Regions 2*, *4* and *6*, which are all sections with considerable variability in shoreline orientation and/or important points of attenuation (refer to Fig. 3).

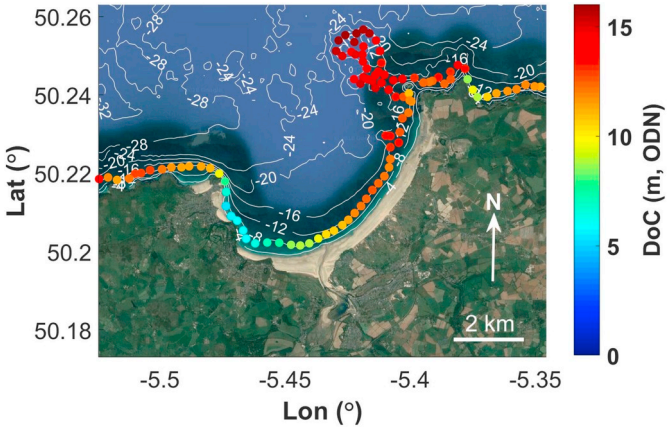

Fig. 7. Example of along-embayment variability in depth of closure due to wave transformation for *Region 2* using $DoC_{param,b}$ (Hallermeier, 1978) (Eq. (1)). (For interpretation of the references to colour in this figure legend, the reader is referred to the web version of this article.)

5.3. DoC determined using bed shear stress maxima (DoC_{stress})

5.3.1. Wave action bed shear stress ($DoC_{stress,a}$)

Wave-induced bed shear stress under the most extreme wave conditions ($H_{s,12}$ and $T_{p,12}$ for $t = 4$ years) was computed along the model domains for the six study regions and presented in Fig. 8 (left panels). Values of wave-induced shear stress are highly variable along the study sites and these are related to the orientation and configuration of the shoreface. Greater values of $\tau_w > 5\,\mathrm{Nm}^{-2}$ at depths from 10 to 20 m occur in west-facing embayments in *Region 1*, *3*, *5* and *6* (Fig. 8a, g, m, p), whereas bed shear stresses are significantly less ($\tau_w < 1\,\mathrm{Nm}^{-2}$) at similar water depths off NE-facing beaches, such as Porthminster and Carbis Bay in *Region 2* (Fig. 8d). Embayments in the north of *Region 4* (e.g., Treyarnon) and many beaches in *Region 5* are very energetic and present values of $\tau_w = 4.8\,\mathrm{Nm}^{-2}$ even in 28 m water depth (Fig. 8m). Interestingly, similar values for τ_w to the exposed west-facing embayments are registered in 28 m water depth ($\tau_w \sim 3.5\,\mathrm{Nm}^{-2}$) in several other NE-facing embayments (e.g., Mother Ives and Harlyn in *Region 4*; Fig. 8j). This is attributed to the morphological configuration of these embayments: they are fronted by a short rocky shelf (c. 700 m) that limits wave energy dissipation during wave transformation and refraction.

Computed wave-induced bed shear stress (τ_w) values are compared to the different case scenarios for sediment transport and bedform activity for the three different sediment sizes (Table 2). Wave-induced bed shear stresses exceeding the upper-plane bed transition are presented in Fig. 8 (blue line, right panels) as the nearshore sediment transport under such stresses is considered most relevant in shaping the lower shoreface. For *Region 1*, this threshold occurs in depths > 30 m along the exposed northern part of the embayment, but decreases to ~12 m at the more sheltered southern end, resulting in an average threshold depth of 19 m (blue line, Fig. 8c). In *Region 2*, the location of the upper-plane bed threshold is spatially highly variable with significantly smaller values of 10 m at the southern end, areas where this threshold is not exceeded at all (e.g., Porthminster and Carbis Bay), and a more exposed section with values > 28 m (e.g., Godrevy and Gwithian, blue line, Fig. 8f). Embayment-averaged values for the transition depth are generally inflated due to the maximum transition depth values associated with the headlands, which often have values of ~30 m. In the more alongshore-uniform *Regions 3* and *4* (blue line, Fig. 8i, l), the isobath for the upper-plane bed transition is 22 m and 25 m, respectively. Values for the embayments within these regions are generally around 18–20 m for *Region 3* and close to 25 m for *Region 4*, while values are > 28 m around the headlands. In *Region 5*, the depth for the transition to upper-plane bed is largest and is near-constant (> 29 m, Fig. 8o). Finally, in *Region 6* (Fig. 8r), the transition depth closely follows the 20-m contour line (Saunton, Croyde and Woolacombe), and decreases to 10 m water depth in the south due to wave dissipation by a point of refraction located in the south of the region.

The results are strongly dependent on the sediment size selected for the calculations ($D_{50} = 0.3$ mm in our case) as shown in Fig. 9a. For a sediment size of 0.15 mm the threshold isobaths tend to be > 18 m larger than for medium sand (not shown), while for the case of the coarser sediment ($D_{50} = 0.6$ mm), the transition to upper-plane bed is only observed up to 12 m in one of the six domains (*Region 5*, light blue line in Fig. 9a). Results for the less energetic of scenarios (sediment motion, initiation of vortex ripples and initiation of post-vortex ripples) are not presented as the three associated sediment transport thresholds τ_{cr} (for all the considered D_{50}) are exceeded throughout all study

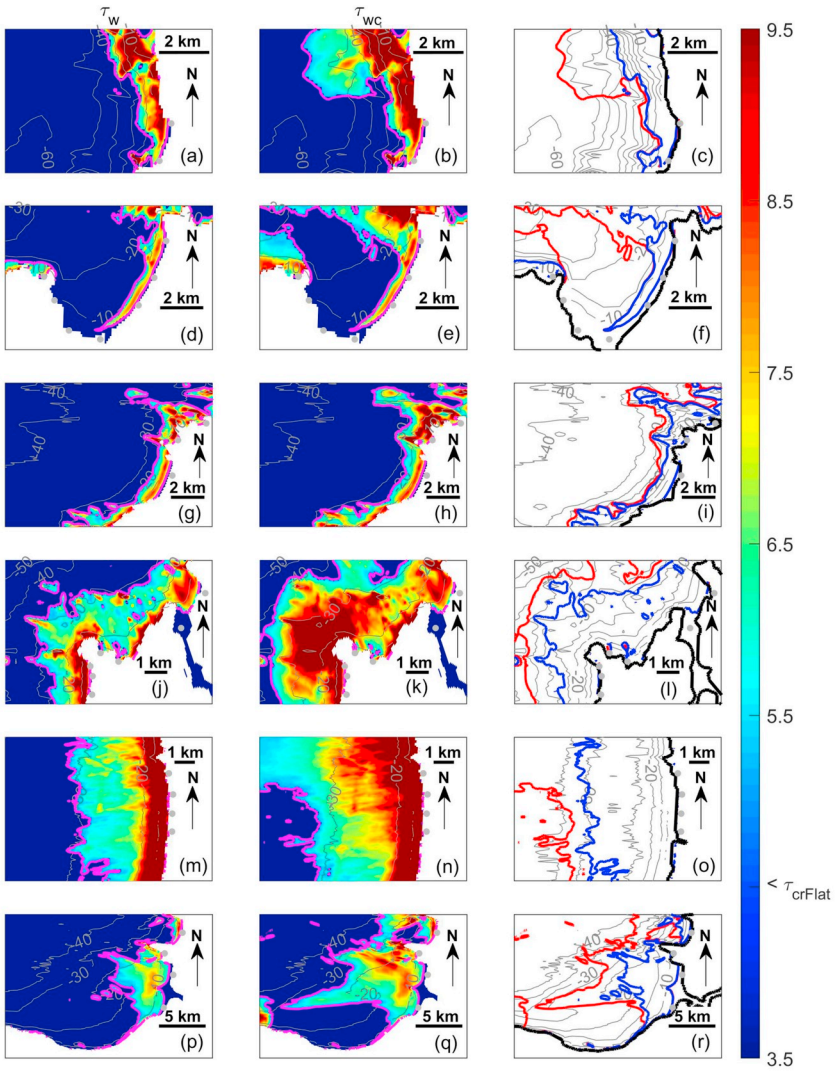

Fig. 8. Left panels show wave-induced bed shear stress (τ_w) computed for extreme wave conditions ($H_{s,12}$ and $T_{p,12}$) and for *Regions 1–6* (a, d, g, j, m, p). Middle panels present combined wave- and current-induced bed shear stress (τ_{wc}) computed for extreme wave conditions ($H_{s,12}$ and $T_{p,12}$) during maximum values of tidal currents (spring tides) and for *Regions 1–6* (b, e, h, k, n, q). Magenta line represents the bed shear stress at the transition to upper-plane bed conditions for medium sand (D_{50} = 0.3 mm, τ_{cr} = 4.77 Nm^{-2}). Right panels: τ_w (blue) and τ_{wc} (red) transition depth to upper-plane bed conditions. (For interpretation of the references to colour in this figure legend, the reader is referred to the web version of this article.)

Table 2
Dependence of critical shear stress values (Nm^{-2}) with sediment size for the considered scenarios: sediment motion, initiation of vortex ripples, initiation of post-vortex ripples and plane bed.

		D_{50} (mm)		
		0.15	0.3	0.6
Bedform activity	Sediment motion	0.17	0.34	0.69
	Initiation of vortex ripples	0.24	0.48	0.95
	Initiation of post-vortex ripples	0.48	0.95	1.91
	Transition to plane bed	2.39	4.78	9.55

regions (depths > 50 m).

5.3.2. *Wave and tidal current bed shear stress ($DoC_{stress,b}$)*

On a high-energy and macrotidal coast, it is important to assess the influence of tidal currents on the bottom stress, in addition to wave agitation, as an additional mobiliser and transporter of sediment. Accounting for the effect of tidal motion on the depth of closure is a prime motivation and novel aspect of this study. The occurrence of combined wave and current bed shear stress (τ_{wc}, $DoC_{stress,b}$) exceeding critical values for transition to upper-plane bed across all study regions is presented in Fig. 8 (middle panels). During extreme conditions (storms and spring tides), sheet flow occurs in all the studied LTEs. Maximum depths in the central part of the embayments that register such extreme flows are 20–30 m, and these values are very similar to those obtained computing only wave-induced bed shear stress (red and blue lines in Fig. 8, right panels). The contribution of the tidal currents in the computed total shear stresses in the central section of the embayments is small (< 0.34 Nm^{-2}) for the case of *Regions 1–3* (Fig. 8c, f, i). However, significant increases in τ_{wc} relative to τ_w are evident around headlands due to stronger tidal currents at these locations (Fig. 8c, f, i). Accounting for tidal currents results in an increase of the depth affected by sheet flow of c. 1 m for wide and W-facing LTEs (Fig. 8b, h) and in excess of 5 m for short LTEs with variable orientation (Fig. 8e, k) as these latter settings are highly influenced by the tidal currents around headlands. Additionally, the maximum limit of sheet flow for combined wave and current bed shear stress increases *O*(10 m) with respect to τ_w in embayments affected by large tidal range (MSR = 7–8, Fig. 8q).

The maximum depths of sediment transport (*DoC-motion*, Eq. (2)) determined for offshore wave values ($DoC_{param,a}$) are compared with the region-averaged depth values for sediment motion, initiation of vortex ripples, initiation of post-vortex ripples and transition to plane bed ($DoC_{stress,b}$). The depths of sediment motion, initiation of vortex ripples and initiation of post-vortex ripples under extreme conditions are exceeded across the entire domain for the six regions, and are significantly larger than the parameterized *DoC-motion*. On the other hand, the *DoC-motion* depths correspond closely to the upper-plane bed transition

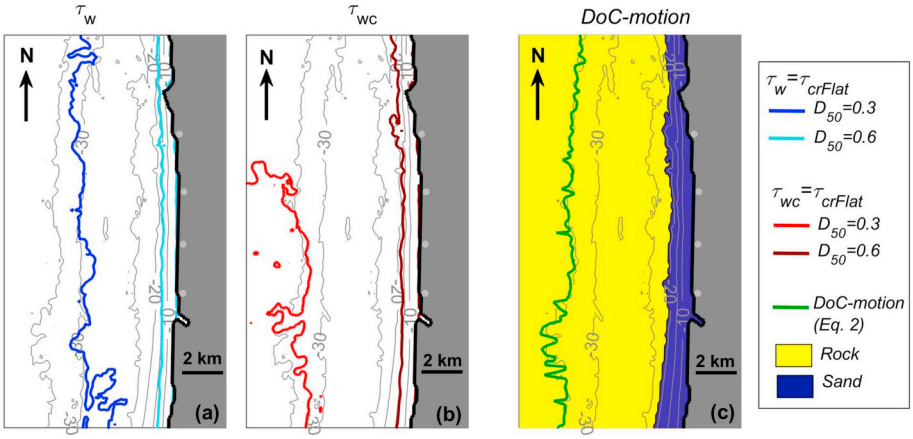

Fig. 9. Bed shear stress at the transition to upper-plane bed conditions for medium and coarse sand (D_{50} = 0.3 and 0.6 mm), limit for initiation of motion and depth between sand and rock for *Region 5*. Bed shear stress transition limit is computed using (a) wave-induced bed shear stress (τ_w) and (b) combined wave- and current-induced bed shear stress (τ_{wc}) computed for extreme wave conditions ($H_{s,12}$ and $T_{p,12}$) and maximum tidal currents (spring tides). (c) *DoC-motion* is predicted using Hallermeier (1981) (Eq. (2)), and depth between sand-rock is based on observations. (For interpretation of the references to colour in this figure legend, the reader is referred to the web version of this article.)

Table 3
Summary of results for the predicted shoreface limits along the SW of England. Region-averaged values of *DoC*, *DoC-motion*, sand-rock transition depth, *DoT* and associated along-coast standard deviation (*SD*) using the different formulations are presented

	$DoC_{obs,a}$	$DoC_{obs,b}$	$DoC_{param,a}$				$DoC_{param,b}$						DoC_{stress}			
	DoC (m)	*Transition depth (m)*	*DoC-motion (m)*	*DoC (m)*			*DoC (m)*						*DoT (m)*			
Region	*SD* ≤ 0.14	*Sand – rock*	Eq. 2 *Hall.*	Eq. 1 *Hall.*	Eq. 4 *Cap.*	Eq. 3 *Bir.*	Eq. 2 *Hall.*	*SD*	Eq. 4 *Cap.*	*SD*	Eq. 3 *Bir.*	*SD*	$\tau_w > \tau_{crFlat}$	*SD*	$\tau_{wc} > \tau_{crFlat}$	*SD*
1	–	12.9	50.1	23.3	17.6	17.5	13.1	1.8	11.8	1.7	9.9	1.3	19	5	22	9.5
2	–	23.1	46.4	21.1	16.2	15.9	9.8	1.6	9.6	1.5	10.1	1.1	0-15	6	0-20	5
3	–	22.5	40.6	20.2	16.3	16.1	13.3	1.6	11.8	1.4	10.0	0.7	22	6	35	5
4	–	21.1	39.4	19.3	15.0	14.6	14.6	1.3	13.1	1	11.1	1.5	28	5	38	5
5	–	21.7	35.2	19.0	14.9	14.2	16.5	0.6	14.9	0.3	12.9	0.3	29	2	35	2
6	–	> 30	33.7	18.8	14.8	14.3	14.3	1.9	10.7	0.7	6.8	0.9	19	5	30	4
Perranporth	14.5	26*	40.6	20.2	16.3	16.1	14.4	0.4	13.1	0.4	10.8	0.6	22	3	28	5

* This value corresponds with significant textural change on the seabed.

during storm conditions, or the maximum depth of significant potential sediment transport (*DoT*) computed using the process-based method ($DoC_{stress,b}$), for *Regions 3*, *4*, *5* and *6* (see Fig. 9b–c and Table 3). This suggests that *DoC-motion* is more representative of the transition to upper-plane bed conditions than of maximum depth of sediment motion under the influence of maximum wave and tidal shear stresses for highly energetic and macrotidal coastlines.

6. Discussion

To facilitate discussion of the different *DoC* estimates obtained using the multi-criteria approach, a summary of the results is presented in Table 3. Comparing the various applied *DoC* formulations provides insights into the usefulness of the different approaches and reinforces the notion that depth of closure is a theoretical concept that will vary according to the used definition. The most widely-used definition for depth of closure proposed by Hallermeier (1978), Birkemeier (1985) and Capobianco et al. (1997) is the basal limit of the envelope of profile change or *DoC*. When the inshore wave conditions are used ($DoC_{param,b}$), the results correspond with shallow values (10–15 m) and are very similar to the limit of significant change using the observational dataset for the case of Perranporth ($DoC_{obs,a}$) for Hallermeier (1978). In contrast, *DoC* values computed using Capobianco et al. (1997) and Birkemeier (1985) for inshore wave conditions are always O(1–2 m) below the observations. Hallermeier (1981) also defined an outer limit (*DoC-motion*) as the offshore boundary of the wave-constructed profile. The latter should correspond with the deepest isobath where sediment motion occurs, but analysis of modelled wave and current bed shear stresses ($DoC_{stress,b}$) reveals that this depth corresponds best with the upper-plane bed limit ($\tau_{wc} > \tau_{crFlat}$, Table 3) under extreme wave conditions, or *DoT*. Furthermore, observations of seabed type distribution ($DoC_{obs,b}$) also suggest that significant sediment exchange under high energy conditions (in this case the winter of 2016) is possible at those isobaths. Consequently, some authors such as Wright (1987, 1995) also considered this deeper limit of extreme motion as a boundary of significant bed-level change, justifying that vertical fluctuations of several cm's (i.e., below the survey accuracy used for defining *DoC*) can represent large volumes of sediment when they are integrated over a wide and gentle-gradient shoreface.

As identified by Capobianco et al. (1997) and Nicholls et al. (1998b), wave parameterisations (DoC_{param} methods) are highly dependent on the timescale of interest. We used a 4-year time series of wave conditions, which included the most energetic winter affecting the coast of SW England (winter 2013/14) since at least 1948 (Masselink et al., 2015); this allows a consideration of the predicted *DoC* values over at least the decadal time scale. If $H_{s,12}$ and $T_{p,12}$ are derived from the complete 4-year time series, the *DoC* values are c. 4 m larger than if $\langle DoC \rangle$ is used (yearly-averaged *DoC* computed using $H_{s,12}$ and $T_{p,12}$ for each year in the time series). As the concept of depth of closure is generally related to shoreface variability over inter-annual to decadal time scale, it is advisable to select the longest wave time series possible to estimate *DoC*. Furthermore, *DoC* parameterisations (DoC_{param}) suggest that this value will increase over time, moving towards the maximum depth of significant sediment transport, or *DoT*.

Previous studies have identified the influence of geological control on the closure depth (Robertson et al., 2008; Ortiz and Ashton, 2016) and, hence, the necessity to use inshore wave conditions when estimating the active shoreface in embayed coastlines (Kraus et al., 1998). Accordingly, we found that using inshore wave conditions ($DoC_{param,b}$) is more appropriate along embayed coastlines, especially for stretches

of coastline not directly facing the prevailing wave direction and/or protected by protruding headlands. However, the closure depth computed using the inshore wave conditions depends on the water depth from which the wave height is extracted: the shallower the depth, the smaller the waves, and the lower the *DoC* value. The inshore wave height and associated period extracted at the actual predicted *DoC* are used here, obtained through an iterative method, yielding *DoC* values that vary along the embayment as a result of the spatial gradient in the wave conditions affecting it.

Similar to the results presented in Robertson et al. (2008), the depth of closure formulation proposed by Hallermeier (1978) (Eq. (1)) provides the best matching with the morphologic observations ($DoC_{obs,a}$, and a closure criteria of *O*14cm defined by the field data collection uncertainty, Table 3) and the procedure to compute this depth closure estimate is as follows: (1) $H_{s,12}$ and $T_{p,12}$ are computed using the wave time series that encompasses the shoreface monitoring period; (2) the offshore wave conditions are transformed into intermediate/shallow water; (3) the modelled inshore sea state in several representative profiles of the embayment is inserted into Eq. (1) and the embayment-averaged closure depth is computed; and (4) the depth of closure value is considered relative to MLWS and then corrected to the survey datum.

As pointed out by Wright (1987), Pilkey et al. (1993), Cowell et al. (2003), and Ortiz and Ashton (2016), the active shoreface is deeper than often predicted using observations and wave-based parameterisations. Recently, Ortiz and Ashton (2016) explored the shoreface dynamics at several locations on the East coast of the U.S. and concluded that $DoC_{param,b}$ methods under-predict the morphodynamic closure depth. Similarly, our study shows that, in all cases, modelled bed shear stresses for the transitional limits of bedform activity (DoC_{stress}) are significantly deeper than those computed using the wave parameterisations ($DoC_{param,b}$, Table 3). Computed bed shear stresses, reinforced by seabed type distribution observations ($DoC_{obs,b}$), suggest that wave currents during extreme storm events ($H_{s,12}$ and $T_{p,12}$) can induce energetic sediment transport well seaward of the limit of 'significant' morphological change or *DoC* (where 'significant' is associated to the minimum detectable limit by the instrumentation) as $DoT \gg DoC$. During these events, the wave orbital velocities across the shoreface suggest that under such conditions most of the embayments experience extreme sediment motion, leading to upper-plane bed conditions, up to large depths (> 35 m, Table 3) even when disregarding tidal action. These results are similar to the values for Southeastern Australia (Wright, 1976; Wright, 1995), or the outcomes shown in Wright et al. (1986) and Wright (1987) for the Middle Atlantic Bight, where the limit for on/offshore sediment transport in these microtidal and energetic shelves exceeds the 30-m isobaths. When also considering tidal currents during the maximum flood in a tidal cycle, this transition depth can increase by > 5 m in areas where coastal geometry and bottom topography (e.g., headlands) induce maximum flow speeds.

Fig. 10 synthesises how the maximum depth of sediment transport (*DoT*) varies as a function of wave height and tidal current velocity. The results are obtained using the process-based method (computation of bed shear stresses due to waves and tidal currents, $DoC_{stress,b}$) for transition to upper-plane bed (extreme sediment motion). Traditionally, the *DoC* concept is limited to wave-dominated coastlines where tidal currents do not significantly affect sediment transport; however, Fig. 10 represents a combined approach to the issue and can be applied to environments where strong tidal currents are important and waves are not the sole sediment-stirring factor. As can be observed in the figure, whilst keeping H_s constant, *DoT* increases with increasing tidal current velocity and/or increasing wave period. Due to the concurrence of a high-energy wave climate and strong tidal currents, *DoT* thresholds along the southwest coast of England (30–50 m) are relatively large compared to most other environments (Fig. 10). Moderately energetic shelves (e.g., East coast of England; EE) with large tidal currents can exhibit values for the offshore limit of the active shoreface that are similar to microtidal and more energetic coastlines (Middle Atlantic Bight; MAB). A comparison between the coast of SW England (high energy, macrotidal) to New South Wales, Australia (high energy, microtidal), indicates that *DoT* values are c. 10 m deeper in the SW England, due to the presence of greater tidal currents.

During extreme storm events, exposed embayments can experience cross-shore sediment transport that exceeds the depth of the base of headlands, allowing sediment to move a considerable distance seaward of the beach-constraining headlands. Furthermore, along a macrotidal coast, the shoreface area that is morphodynamically active during these storm events will increase due to the contribution of the tidal currents to the total bottom shear stress, especially during spring tides. A conceptual model of the shoreface dynamics for an idealised high-energy and macrotidal coast that illustrates this situation is presented in Fig. 11. The implication is that, even though the headlands that flank many embayed beaches appear sufficiently prominent to suggest that the embayed beach can be considered a closed cell (with restricted sediment transport in/out the cell), significant sediment transport at a short time-scale may take place well beyond the ends of the headland, leading to headland bypassing. Some recent studies also point in this direction, demonstrating that cell compartments often includes several embayed beaches (Kinsela et al., 2017; McCarroll et al., 2018) and that transport of sediment under extreme events is likely to occur even around headlands with an apex that reaches the 50-m isobath (George, 2016). This challenges the notion that embayed beaches are generally closed cells and that headland bypassing may be more widespread than commonly assumed. Accordingly, a re-evaluation of the concept of closed embayments is especially appropriate for the north Cornish coastline, as these embayments can be deemed opened cells, and indeed, the coast of SW England as a whole can perhaps be considered a single sediment cell from Land's End to the Bristol Channel, as previously suggested by May and Hansom (2003).

7. Conclusions

This paper revisits the 'depth of closure' (*DoC*) concept through the study of the predicted zone of significant sediment transport and evaluates its applicability to the macrotidal and exposed coastline of SW England, discussing the implications for headland bypassing and exploring the open/closed cell concept along embayed coastlines. Two main closure limits based on shoreface morphodynamics and seabed activity are considered: the widely-used morphological depth of closure (*DoC*) defined as the basal limit of the envelope of profile change, and a deeper limit of maximum depth of 'significant' sediment transport (*DoT*) under extreme events, where 'significant' refers to intense bed agitation represented by the upper-plane bed transition. The key findings are:

1. *DoT* is considered a boundary of significant bed level change as up to that water depth intense sediment transport takes place (upper-plane bed transition). Although over the medium-term time scale (years) these morphological changes might not be detectable (below the survey accuracy), they are likely to represent large volumes of sediment when integrated over the shoreface.
2. Along embayed coastlines, inshore wave conditions (using the longest time series possible) must be used to compute *DoC*, as offshore wave conditions are not representative due to wave transformation processes. Wave attenuation, refraction and diffraction around headlands can result in a large spatial gradient in the inshore wave conditions, and the local embayment geometry can have a greater impact on *DoC* values than any regional variability in wave exposure.
3. The wave-based parameterisation of depth of closure by Hallermeier (1978) (Eq. (1)) provides a good approximation of observed morphological depth of closure (for a minimum detectable limit of 0.14 m) at the medium-term scale for the exposed and macrotidal study area, if calculated relative to MLWS.

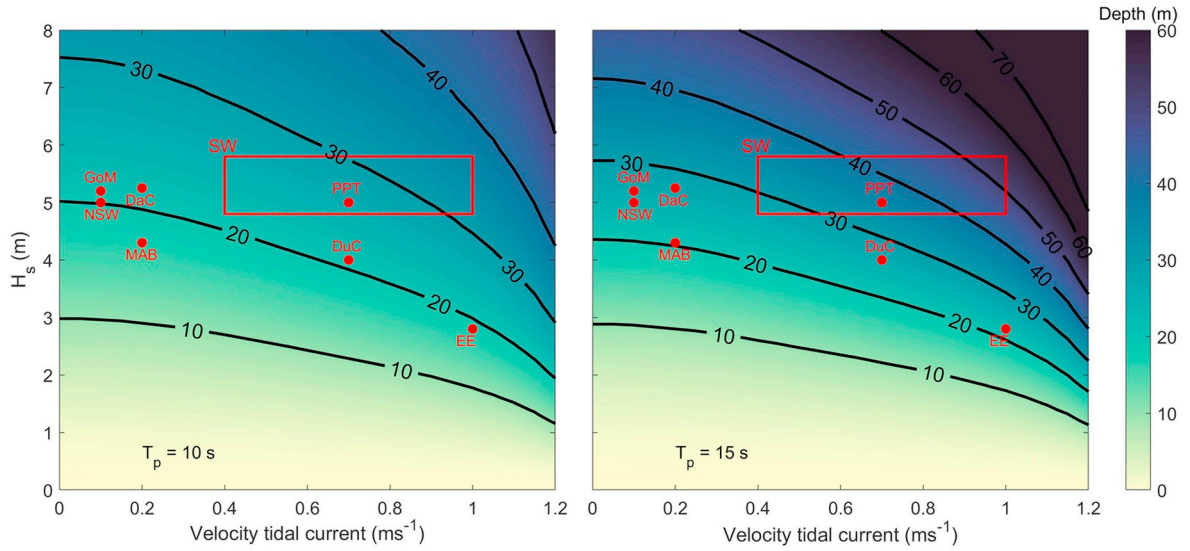

Fig. 10. Variation of *DoT* across a broad wave-current parameter space. *DoT* is computed using significant wave height (H_s) and tidal current speed ($\overline{U}$) for medium sand (D_{50} = 0.3 mm) and a constant period (T_p) of 10 s (left panel) and 15 s (right panel). Examples of computed *DoT* values using extreme significant wave height ($H_{s,99\%}$) and maximum tidal current in the bottom layer are shown as red dots: *GoM* – Gulf of Mexico (Pepper and Stone, 2004; Ortiz and Ashton, 2016); *NSW* – New South Wales (Kulmar et al., 2005); *MAB* – Middle Atlantic Bight (Wright et al., 1994); *DaC* – Danish Coast (Aagaard et al., 2010); *DuC* – Dutch Coast (Luijendijk et al., 2017); *EE* – East England (Haskoning, 2005; Leonardi and Plater, 2017); and *PPT* – Perranporth. The range of H_s – $\overline{U}$ combinations estimated for the SW (South West England) is also indicated (red box). (For interpretation of the references to colour in this figure legend, the reader is referred to the web version of this article.)

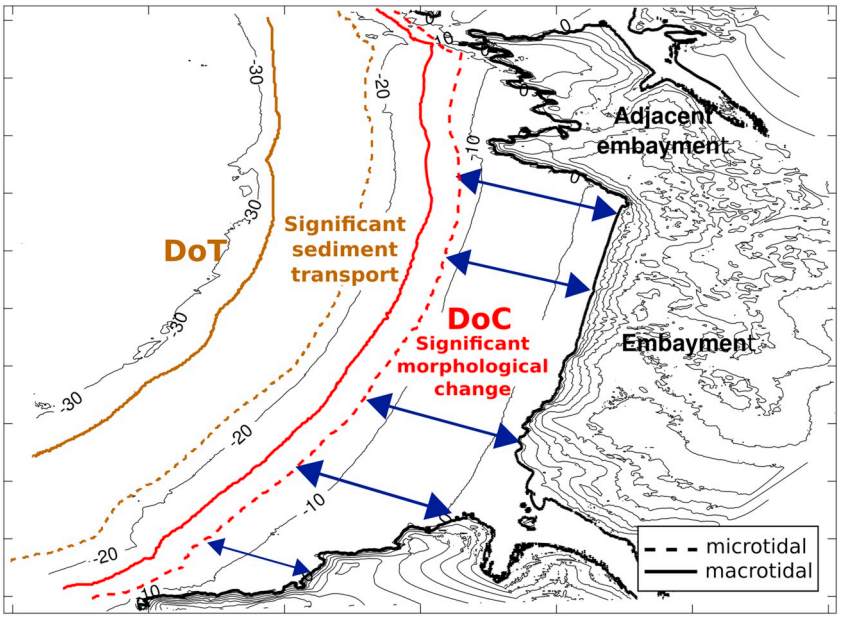

Fig. 11. Plan view of an idealised high-energy and embayed coastline. (For interpretation of the references to colour in this figure legend, the reader is referred to the web version of this article.)

4. The active shoreface is deeper than often considered by engineering practice. Combined wave-tide bed shear stresses computed following a process-based method, reinforced by seabed type distribution observations, suggest that important sediment transport during extreme conditions occurs well seaward of the limit of 'significant' morphological change.
5. *DoT* is computed across a broad wave height and (tidal) current velocity parameter space to investigate the influence of currents on wave-derived values for maximum depth of significant transport at a range of contrasting coastal locations. *DoT* depths can be increased by ~10 m *O*(30%) for macrotidal locations compared to microtidal environments with a similar wave climate, highlighting the importance of considering tidal currents in realistic *DoT* calculations.
6. The considerable depth (≫30 m) at which combined wave- and tide-driven sediment transport can occur under extreme wave conditions along exposed, macrotidal and embayed settings implies that transport of fine and medium sediment under extreme events can exist around headlands with an apex base that surpasses the 30-m isobath. This significantly increases the potential for headland bypassing and challenges the notion that embayments are generally considered closed sediment cells.

Acknowledgments

This work was supported by UK Natural Environment Research Council grant (NE/M004996/1; BLUE-coast project). This study is only possible thanks to the efforts of the members of the Coastal Process Research Group who have been, and still are, collecting observations at Perranporth. The UK MetOffice (Dr Andy Saulter) and Channel Coast Observatory are project stakeholders and kindly provided modelled wave data and measured topography, respectively. We would also like to acknowledge the ESPRC-funded ARCC "Adaptation and Resilience of Coastal Energy Supply" (ARCoES) project (EPSRC EP/I035390/1) for providing the FVCOM modelled current data.

References

Aagaard, T., Kroon, A., Greenwood, B., Hughes, M.G., 2010. Observations of offshore bar decay: sediment budgets and the role of lower shoreface processes. Cont. Shelf Res. 30 (14), 1497–1510.

Aragones, L., Serra, J.C., Villacampa, Y., Saval, J.M., Tinoco, H., 2016. New methodology for describing the equilibrium beach profile applied to the Valencia's beaches. Geomorphology 259, 1–11.

BERR, 2008. Atlas of UK Marine Renewable Energy Resources. Tech. Rep.

Birkemeier, W., 1985. Field data on seaward limit of profile change. J. Waterw. Port Coast. Ocean Eng. 598–602.

Booij, N., Ris, R.C., Holthuijsen, L.H., 1999. A third-generation wave model for coastal regions: 1. Model description and validation. J. Geophys. Res. 104 (C4), 7649–7666.

Capobianco, M., Larson, M., Nicholls, R.J., Kraus, N.C., 1997. Depth of closure: a contribution to the reconciliation of theory, practise and evidence. In: Proceedings of Coastal Dynamics. ASCE, New York, pp. 506–515.

Capobianco, M., Hanson, H., Larson, M., Steetzel, H., Stive, M.J.F., Chatelus, Y., Aarninkhof, S., Karambas, T., 2002. Nourishment design and evaluation: applicability of model concepts. Coast. Eng. 47 (2), 113–135.

Chen, C., Liu, H., Beardsley, R.C., 2003. An unstructured, finite-volume, three-dimensional, primitive equation ocean model: application to coastal ocean and estuaries. J. Atmos. Ocean. Technol. 20 (1), 159–186.

Chesher, J.A., Smythe, D.K., Bishop, P., 1981. The Geology of the Minches, Inner Sound and Sound of Raasay. rep. inst. Edition. pp. 41.

Cowell, P.J., Stive, M.J.F., Niedoroda, A.W., de Vriend, H.J., Swift, D.J.P., Kaminsky, G.M., Capobianco, M., 2003. The coastal-tract (part 1): a conceptual approach to aggregated modeling of low-order coastal change. J. Coast. Res. 19 (4), 812–827.

De Dominicis, M., O'Hara Murray, R., Wolf, J., 2017. Multi-scale ocean response to a large tidal stream turbine array. Renew. Energy 114, 1160–1179. https://doi.org/10.1016/j.renene.2017.07.058.

Dott, R.H., Bourgeois, J., 1982. Hummock stratification: significance of its variable bedding sequences. Geol. Soc. Am. Bull. 93 (August), 663–680.

George, D.A., 2016. Circulation and Sediment Transport at Headlands With Implications for Littoral Cell Boundaries. Ph.D. thesis. University of California, Davis.

Grant, W.D., Madsen, O., 1982. Movable bed roughness in unsteady oscillatory flow. J. Geophys. Res. 87, 469–481.

Hallermeier, R.J., 1978. Uses for a calculated limit depth to beach erosion. In: Proceedings of the 16th Coastal Engineering Conference. ASCE, New York, pp. 1493–1512.

Hallermeier, R.J., 1981. A profile zonation for seasonal sand beaches from wave climate. Coast. Eng. 4 (C), 253–277.

Hands, E.B., Allison, M.C., 1991. Mound migration in deeper water and methods of categorising active and stable depths. In: Proceedings of the ASCE Specialty Conference on Quantitative Approaches to Coastal Sediment Processes. vol. 2. pp. 1985–1999.

Hanson, H., Kraus, N.C., 1989. GENESIS: Generalized Model for Simulating Shoreline Change. Tech. rep. 1. Coastal Engineering Research Center, U.S. Army Corps of Engineers, Vicksburg, Mississippi.

Hartman, M., Kennedy, A.B., 2016. Depth of closure over large regions using airborne bathymetric lidar. Mar. Geol. 379, 52–63.

Haskoning, 2005. Suffolk wave and tide analysis report. Final report 9R0839/R/PBor. In: Report for the Environment Agency, Anglian Region. Royal Haskoning, Peterborough (December 2005).

Hinton, C., Nicholls, R.J., 1998. Spatial and temporal behaviour of depth of closure along the Holland coast. In: 26th International Conference on Coastal Engineering, pp. 2913–2925.

Kinsela, M.A., Morris, B.D., Linklater, M., Hanslow, D.J., 2017. Second-pass assessment of potential exposure to shoreline change in New South Wales, Australia, using a sediment compartments framework. J. Mar. Sci. Eng. 5 (4), 61. https://doi.org/10.3390/jmse5040061.

Komen, G.J., Hasselmann, S., Hasselmann, K., 1984. On the existence of a fully developed wind-sea spectrum. J. Phys. Oceanogr. 14, 1271–1285.

Kraus, C., Larson, M., Wise, R., 1998. Depth of closure in beach fill design. In: Proceedings 12th National Conference on Beach Preservation Technology. vol. 40. Florida Shore and Beach Preservation Association, pp. 271–286.

Kulmar, M., Lord, D., Sanderson, B., 2005. Future directions for wave data collection in New South Wales. In: Proceedings of the 17th Australasian Coastal and Ocean Engineering Ports Conference, pp. 167–172 Australia, Sidney.

Larson, M., 1991. Equilibrium profile of a beach with varying grain size. In: Proceedings Coastal Sediments 1991. ASCE, Seattle, pp. 861–874.

Larson, M., Kraus, N.C., 1992. Dynamics of longshore bars. In: Proceedings Coastal Engineering. ASCE, Venice, pp. 2219–2232.

Leonardi, N., Plater, A.J., 2017. Residual flow patterns and morphological changes along macro- and meso-tidal coastline. Adv. Water Resour. 109, 290–301.

Luijendijk, A.P., Ranasinghe, R., de Schipper, M.A., Huisman, B.A., Swinkels, C.M., Walstra, D.J.R., Stive, M.J.F., 2017. The initial morphological response of the Sand Engine: a process-based modelling study. Coast. Eng. 119, 1–14.

Marsh, S.W., Nicholls, R.J., Kroon, A., Hoekstra, P., 1998. Assessment of depth of closure on a nourished beach: Terschelling, the Netherlands. In: 26th International Conference on Coastal Engineering, pp. 3110–3123.

Masselink, G., Scott, T., Poate, T., Russell, P., Davidson, M., Conley, D., 2015. The extreme 2013/2014 winter storms: hydrodynamic forcing and coastal response along the southwest coast of England. Earth Surf. Process. Landf. https://doi.org/10.1002/esp.3836. (n/a–n/a).

May, V.J., Hansom, J.D., 2003. Coastal Geomorphology of Great Britain, Geological edition. Joint Nature Conservation Committee, Peterborough, pp. 754.

McCarroll, J., Masselink, G., Valiente, N.G., Scott, T., King, E., 2018. Wave and tidal controls on headland bypassing and embayment circulation. J. Mar. Sci. Eng. 6 (3), 94. https://doi.org/10.3390/jmse6030094.

Nicholls, R.J., Birkemeier, W.A., Lee, G., 1998a. Evaluation of depth of closure using data from Duck, NC, USA. Mar. Geol. 148 (3–4), 179–201.

Nicholls, R.J., Larson, M., Capobianco, M., Birkemeier, W.A., 1998b. Depth of closure: improving understanding and prediction. In: Proceedings of the Coastal Engineering Conference. vol. 3. ASCE, New York, pp. 2888–2901.

Nichols, G., 1999. Sedimentology and Stratigraphy, Second edition. John Wiley & Sons, Ltd., Publication, Oxford, pp. 419.

Nielsen, P., 1981. Dynamics and geometry of wave-generated ripples. J. Geophys. Res. 86, 6467–6472.

Ortiz, A.C., Ashton, A.D., 2016. Exploring shoreface dynamics and a mechanistic explanation for a morphodynamic depth of closure. J. Geophys. Res. Earth Surf. 121 (2), 442–464.

Pawlowicz, R., Beardsley, B., Lentz, S., 2002. Classical tidal harmonic analysis including error estimates in MATLAB using TTIDE. Comput. Geosci. 28 (8), 929–937.

Pepper, D.A., Stone, G.W., 2004. Hydrodynamic and sedimentary responses to two contrasting winter storms on the inner shelf of the northern Gulf of Mexico. Mar. Geol. 210 (1–4), 43–62.

Peters, S.E., Loss, D.P., 2012. Storm and fair-weather wave base: a relevant distinction? Geology 40 (6), 511–514.

Phillips, M.R., Williams, A.T., 2007. Depth of closure and shoreline indicators: empirical formulae for beach management. J. Coast. Res. 232 (2001), 487–500.

Pilkey, O.H., Young, R.S., Riggs, S.R., Sam Smith, A.W., Wu, H., Pilkey, W.D., 1993. The concept of shoreface profile of equilibrium: a critical review. J. Coast. Res. 9 (1), 255–278.

Plant, N.G., Holland, K.T., Puleo, J.A., 2002. Analysis of the scale errors in nearshore bathymetric data. Mar. Geol. 191 (1–2), 71–86. https://doi.org/10.1016/S0025-3227(02)00497-8.

Potter, P., 1967. Sand bodies and sedimentary environments: a review. AAPG Bull. 51 (3), 337–365.

Prodger, S., Russell, P., Davidson, M., 2016. Grain-size distributions on high-energy sandy beaches and their relation to wave dissipation. Sedimentology 64, 1289–1302.

Robertson, W., Zhang, K., Finkl, C.W., Whitman, D., 2008. Hydrodynamic and geologic influence of event-dependent depth of closure along the South Florida Atlantic Coast. Mar. Geol. 252 (3–4), 156–165. https://doi.org/10.1016/j.margeo.2008.03.018.

Rosati, J.D., Dean, R.G., Walton, T.L., 2013. The modified Bruun Rule extended for landward transport. Mar. Geol. 340, 71–81. https://doi.org/10.1016/j.margeo.2013.04.018.

Roy, P.S., Thom, B.G., 1981. Late Quaternary marine deposition in New South Wales and southern Queensland - an evolutionary model. J. Geol. Soc. Aust. 28 (July), 471–489. https://doi.org/10.1080/00167618108729182.

Samuel, R.M., 2017. Seasonal Variation of Macrobenthos Distribution and the Biophysical Cohesiveness of Sediments on a Macrotidal, Highly Exposed Sandy Beach. Masters Thesis. Faculty of Science and Engineering, Plymouth University.

Saulter, A.J., 2017. Quality Information Document: North West European Shelf Production Centre. NORTHWEST-SHELF ANALYSIS FORECAST WAV 004 012. Tech. Rep. Available at. http://cmems-resources.cls.fr/documents/QUID/CMEMS-NWS-QUID-004-012.pdf.

Scott, T., Masselink, G., Russell, P., 2011. Morphodynamic characteristics and classification of beaches in England and Wales. Mar. Geol. 286 (1–4), 1–20.

Soulsby, R., 1995. Bed shear-stresses due to combined waves and currents. In: Stive, M., de Vriend, H. (Eds.), Advances in Coastal Morphodynamics, (4–20 to 4–23).

Soulsby, R., 1997. Dynamics of Marine Sands: A Manual for Practical Applications. Thomas Telford Publications, pp. 249.

Stive, M.J.F., de Vriend, H.J., 1995. Modelling shoreface profile evolution. Mar. Geol. 126 (1–4), 235–248. https://doi.org/10.1016/0025-3227(95)00080-I.

Stive, M.J., Nicholls, R.J., de Vriend, H.J., 1991. Sea-level rise and shore nourishment: a discussion. Coast. Eng. 16 (1), 147–163.

Stive, M.J., de Vriend, H.J., Nicholls, R.J., Capobianco, M., 1992. Shore nourishment and the active zone: a time scale dependent view. In: Proceedings of the Twenty-Third Coastal Engineering Conference. ASCE, New York, pp. 2464–2473.

Tanaka, H., Van To, D., 1995. Initial motion of sediment under waves and wave-current combined motions. Coast. Eng. 25 (3–4), 153–163.

Thieler, E.R., Pilkey, O.H., Cleary, W.J., Schwab, W.C., 2001. Modern sedimentation on

the shoreface and inner continental shelf at Wrightsville Beach, North Carolina, U.S.A. J. Sediment. Res. 71 (6), 958–970.
Tolman, H.L., 2014. User Manual and System Documentation of WAVE-WATCH III. Tech. Rep.
United Kingdom Hydrographic Office, 2011. INSPIRE Portal & Bathymetry DAC. Available at. http://aws2.caris.com/ukho/mapViewer/map.action.
Work, P.A., Dean, R.G., 1991. Effect of varying sediment size on equilibrium beach profiles. In: Proceedings Coastal Sediments. ASCE, Seattle, pp. 891–904.
Wright, L.D., 1976. Nearshore wave-power dissipation and the coastal energy regime of the Sydney-Jervis Bay region, New South Wales: a comparison. Aust. J. Mar. Freshwat. Res. 27, 633–640.
Wright, L.D., 1987. Shelf-surf zone coupling: diabathic shoreface transport. In: Proceedings of Coastal Sediments. ASCE, Washington, D.C., pp. 25–40.
Wright, L.D., 1995. Morphodynamics of Inner Continental Shelves. CRC Press, Inc.
Wright, L.D., Boon, J.D., Green, M.O., List, J.H., 1986. Response of the mid-shoreface of the southern Mid-Atlantic Bight to a “northeaster”. Geo-Mar. Lett. 6, 153–160.
Wright, L.D., Boon, J.D., Kim, S.C., List, J.H., 1991. Modes of cross-shore sediment transport on the shoreface of the Middle Atlantic Bight. Mar. Geol. 96 (1–2), 19–51.
Wright, L.D., Xu, J.P., Madsen, O.S., 1994. Across-shelf benthic transports on the inner shelf of the Middle Atlantic Bight during the “Halloween storm” of 1991. Mar. Geol. 118 (1–2), 61–77.
Young, I.R., 1999. Wind Generated Ocean Waves. vol. 2 Elsevier Sci, Amsterdam.